

Investigation, modeling, and optimization of cutting parameters in turning of gray cast iron using coated and uncoated silicon nitride ceramic tools. Based on ANN, RSM, and GA optimization

Aissa Laouissi^{1,2}  · M. A. Yallese² · A. Belbah¹ · S. Belhadi² · A. Haddad¹

Received: 29 August 2018 / Accepted: 23 October 2018 / Published online: 5 November 2018

© Springer-Verlag London Ltd., part of Springer Nature 2018

Abstract

A comparative study is undertaken in terms of the surface roughness criterion (R_a), the tangential cutting force (F_z), the cutting power (P_c), and the material removal rate (MRR) in turning of EN-GJL-250 cast iron using both coated and uncoated silicon nitride ceramics (Si_3N_4). The experimental procedure is carried out according to L27 Taguchi design process, and the analysis of variance ANOVA approach used to identify the cutting parameters that most influence the responses gathered. The artificial neural network approach (ANN) and the response surface methodology (RSM) were adopted to developing the mathematical prediction models applied in the optimization procedure that used genetic algorithm (GA). The predictive capabilities of the ANN and RSM models were further compared in terms of their mean absolute deviation (MAD), mean absolute error in percent (MAPE), mean square error (RMSE), and coefficient of determination (R^2). It has been found that the ANN method provides more precise results compared to those of the RSM approach. Moreover, the coated ceramic tool has been found to lead to a better surface quality and a minimum cutting force compared to those obtained by uncoated ceramic. The wear tests undertaken show that, when the flank wear reaches the admissible value of $[V_b] = 0.3 \text{ mm}$, the ratios (tool life C_{1690} /tool life C_{6090}), $(R_a C_{1690}/R_a C_{6090})$, and $(F_z C_{1690}/F_z C_{6090})$ are found to equal 0.88, 1.4, and 0.94, respectively.

Keywords ANOVA · Surface roughness · Cutting force · RSM · ANN · Ceramic · GA

1 Introduction

Metal cutting is a complex process which has numerous factors among whom the cutting forces that lead to following up the

condition of the cutting tool along with the estimation of its service life. They also contribute to the prediction and the thermal analysis of the necessary cutting power, and can finally provide useful information concerning the physical behavior in the

Highlights

ANN is a very robust method for prediction the cutting parameters.
RSM is a very good method for classification and identification.
ANN and RSM methods as they seem to be complementary.
GA optimization can compromise between various responses.
The ratio of the full tests $R_a C_{1690}/R_a C_{6090} \approx 0.88$.
The ratio of the tool life $C_{1690}/\text{tool life } C_{6090} \approx 1.4$.
The 3D topographies is an important investigation tool for surface roughness.

✉ Aissa Laouissi
Aissou_011@yahoo.fr; Laouissi.aissa@univ-guelma.dz

A. Haddad
akhhaddad@gmail.com

M. A. Yallese
yallese.m@gmail.com

¹ Département de Génie Mécanique, Laboratoire de Mécanique Appliquée des Nouveaux Matériaux (LMANM), Université 8 Mai 1945, BP 401, 24000 Guelma, Algeria

A. Belbah
ahmedbelbah@gmail.com

² Département de Génie Mécanique, Laboratoire Mécanique et Structure (LMS), Université 8 Mai 1945, BP 401, 24000 Guelma, Algeria

S. Belhadi
belhadi23@gmail.com

cutting zone. The surface roughness remains the major indicator of surface quality, and consequently one of the most specified customer requirements. Both the cutting forces and the surface roughness are influenced by several parameters linked to the geometry of the cutting tool (nose radius, cutting angles, etc.), the cutting conditions (cutting speed, feeds rate, and cutting depth), the nature of the cutting material, the tool coatings, and the cooling approach [1–3].

The knowledge of the impact of these parameters on the cutting forces and the surface roughness requires the design of the manufacturing process along with the development of the mathematical prediction models that would lead to determining the optimal cutting conditions. Modeling and optimization of cutting parameters are therefore the necessary steps in the manufacturing process that prompted many researchers in recent years to develop and investigate diverse experimentally based models such as the response surface methodology (RSM) [4–6], the artificial neural networks approach (ANN) [5, 6], and the adaptive neuro fuzzy inference system (ANFIS) [7–9]. The response surface methodology is widely used to examine and optimize operational variables. It is efficient in generating a response surface on a particular region of interest, and optimizing responses or designating the operating conditions necessary to achieve the target specifications imposed by manufacturers [10]. Its major advantage lies in its ability to identify both the parameters and the interactions that influence the response study [10, 11]. It, however, shows a weak behavior when faced to non-linear phenomena and consequently is solely applicable in regular experimental domains [11]. Because of these limitations, other procedures have been explored. Among them, the artificial neural network (ANN) approach is a computer-modeling tool based on artificial intelligence. The ANN is capable of modeling both non-linear inputs and outputs more efficiently than any other technique in terms of precision, simplicity, and speed of treatment [12, 13]. Several studies using RSM and ANN methods have been carried out and been published. Yücel and Günay [14] examined the surface roughness (R_a) along with the cutting forces generated during the turning of two white cast irons with hardnesses of 50 and 62 HRC using CBN and ceramic tools. The authors used both the L18 Taguchi and RSM methods in order to optimize the output parameters. The results obtained show that the feed rate (f) and the cutting depth (ap) are the main parameters influencing the surface roughness (R_a) and the cutting force, respectively. The best roughness found is $R_a = 0.262 \mu\text{m}$ with CBN/cast iron (50 HRC) couple. Fetecau and Stan [15] investigated the effect of the cutting parameters and nose radius on the cutting force and surface roughness when turning PTFE composite using a polycrystalline diamond tool. The ANOVA analysis found that (ap) is the most influential parameter on the cutting force with a contribution

of 50.81%, followed by (f) with a contribution of den 40.53%. The analysis showed also the surface roughness to be greatly influenced by (f) with a contribution of 60.73%, while the nose radius displayed a contribution of only 31.72%. Zhong et al. [16] performed an experimental study with the aim of developing prediction models for the roughness criteria (R_a) and (R_t) using the ANN approach when turning copper and aluminum with coated carbide inserts. The investigation revealed the capability of the ANN models with 7-14-18-2 architecture to predicting R_a and R_t values with an average error of 15.27% and 18.63%, respectively. Mia and Dhar [17] were interested in studying the temperature of the tool-piece interface during the hard turning of AISI 1060 steels by coated carbide insert. The analysis of variance (ANOVA) revealed that the cutting temperature is significantly affected by the material hardness with a contribution of 64.23% followed by the cutting speed and finally the feed rate. Furthermore, the cutting temperature predictive models obtained by RSM and ANN were both found to be acceptable even though those of the ANN approach were found to be better. Nouioua et al. [11] presented a comparative study between the ANN and RSM methods for the dry, wet, and MQL turning of X210Cr10 steel. They concluded that the surface roughness is largely influenced by the feed rate with a contribution of 40.46% to 52.41%. They also identified the depth of cut as the most influential factor on cutting force with a contribution of 72.30% to 75.81%. Finally, the ANN method was found to providing much more precise results (with a mean expected error that does not exceed 0.97) compared to those obtained by the RSM for which the MPE can reach the value of 5.5. Chabi et al. [18] conducted a study on the influence of cutting parameters on surface roughness (R_a), tangential cutting force (F_z), and cutting power (P_c) during POMC polymer turning by applying both the ANN and RSM techniques. The results they obtained showed that the feed rate is the most influential factor on (R_a) with a contribution of 66.41%. Furthermore, the depth of cut was found to be the most influential parameter on (F_z) and (P_c) with contributions of 45.41% and 47.81%, respectively. They were followed by the feed rate with a contribution of 31.09% and 30.5% on (F_z) and (P_c), respectively. Finally, the determination coefficients (R^2) of the mathematical models developed showed the robustness and reliability of the ANN method over its RSM counterpart. Tebassi et al. [19] investigated the surface roughness (R_a) and the tangential cutting force (F_z) when turning the inconel 718 with coated carbide tools. They applied both the RSM and ANN methods, and found out that the determination coefficient (R^2) pertaining to (R_a) and (F_z) obtained by RSM was equal to 0.93 and 0.98, respectively. For the ANN models, they were identified to equal 0.98 and 0.99. Yousuff et al.'s research [20, 21] showed that the RSM

method was very effective in modeling and optimizing of surface roughness during cryogenic mold machining used for biomedical applications. The research performed by Kumar and Chauhan [22] led to conclude that the mathematical prediction models developed by the ANN and RSM approaches may be efficiently used to investigate the influence of the cutting parameters on surface roughness. They also found out that the ANN models generated more errors than the RSM ones.

All the precedent studies are aimed to determining the most precise and robust modeling method that would be able to develop reliable mathematical prediction models that will be exploited for optimization.

The objective of the present work is to experimentally investigate the effects of cutting parameters such as (f , ap , V_c) on surface roughness (R_a), tangential cutting force (F_z), cutting power (P_c), and material removal rate (MRR) when turning gray cast iron EN-GJL-250 by coated and uncoated silicon nitride ceramics (Si_3N_4). The results obtained are then used to develop mathematical prediction models based on artificial neuron networks (ANN) and response surface methodology (RSM). The predictive capabilities of the two approaches are compared in terms of their mean absolute deviation (MAD), absolute mean percentage error (MAPE), mean square error (RMSE), and coefficient of determination (R^2). These models are then used to apply a multi-objective optimization procedure by the genetic algorithm (GA) in order to achieve the optimal cutting conditions. Finally, the evolution of surface roughness, cutting force, and flank wear as a function of the machining time and the surface topography (3D) are considered.

2 Experimental procedure

2.1 Material, work-piece, and tool

The turning experiments involving the roughness and the cutting forces measurements were carried out on EN-GJL-250 cast iron test pieces that are 80 mm in diameter and 400 mm in length. The cast iron is widely used in the industry particularly that related to the automotive production (such as pistons, brake discs, and engine blocks) as well as in mechanical engineering (conveyors, pumps, and gears) and piping. Its main advantages rely on its excellent flow ability and machinability, good wear resistance, and high vibration damping capacity. The EN-GJL-250 cast iron possesses a hardness of 250 HB and a yield strength of 250 MPa. Its chemical composition is shown in Table 1.

The lathe used for the tests is a TOS TRENCIN-SN40C model with a spindle power of 6.6 kW, and the ceramics inserts are coated and uncoated silicon nitride- Si_3N_4 (CC1690 and CC6090, Sandvik). They are removable, square shaped, fixed by flanges, of SNGN 120408T02520

Table 1 Chemical composition of EN-GJL-250 cast iron

	Composition	wt%
C	4%	
Si	2.1%	
Mn	0.76%	
P	0.11%	
Ni	0.03%	
Cu	0.28%	
Cr	0.13%	
Fe	92.35%	
Co	0.003%	
Ti	0.015%	

designation, and mounted on a tool holder of CSDNN25x25M12 designation. A Mitutoyo surftest-201 roughness meter was adopted for the instantaneous measurement of the two roughness criteria (R_a) and (R_z) for each cutting condition. It consists of a diamond point (feeler) with a radius of 5 μm moving on the considered surface. The roughness criteria measurement range is (0.05 to 40 μm) for (R_a) and (0.3 to 160 μm) for (R_z). To achieve more accuracy and eliminate errors, all the roughness measurements were obtained directly on the same machine without dismantling the workpiece. Moreover and to better visualize the roughness of the machined surfaces, an AltiSurf® 500 optical metrology device was also used. It allows a fine study of the 3D topography of the machined surfaces. The measurement of the amplitude of the cutting forces was carried out through a KISTLER platform connected to an amplifier and processed through a specialized software. The experimental apparatus is shown in Fig. 1.

2.2 Experimental design

A Taguchi design L_{27} is applied to the experiment planning. Selected input factors and their levels are shown in Table 2. The ranges of the cutting parameters are chosen according to the recommendations of the manufacturer of the cutting tools (i.e., Sandvik).

3 Results and discussion

Table 3 presents the cutting conditions represented by V_c , f , and ap along with the experimental results illustrated by R_a , F_z , and MRR according to the L27 Taguchi design exhibited earlier. In this table, R_a varies between 0.45 and 1.86 μm , while F_z fluctuates between 30.73 and 349.77 N. Finally, the range of variation of P_c and MRR is found to be between 197.513 and 2710.68 W for P_c and between 5200 and 79,500 mm^3/min for MRR.

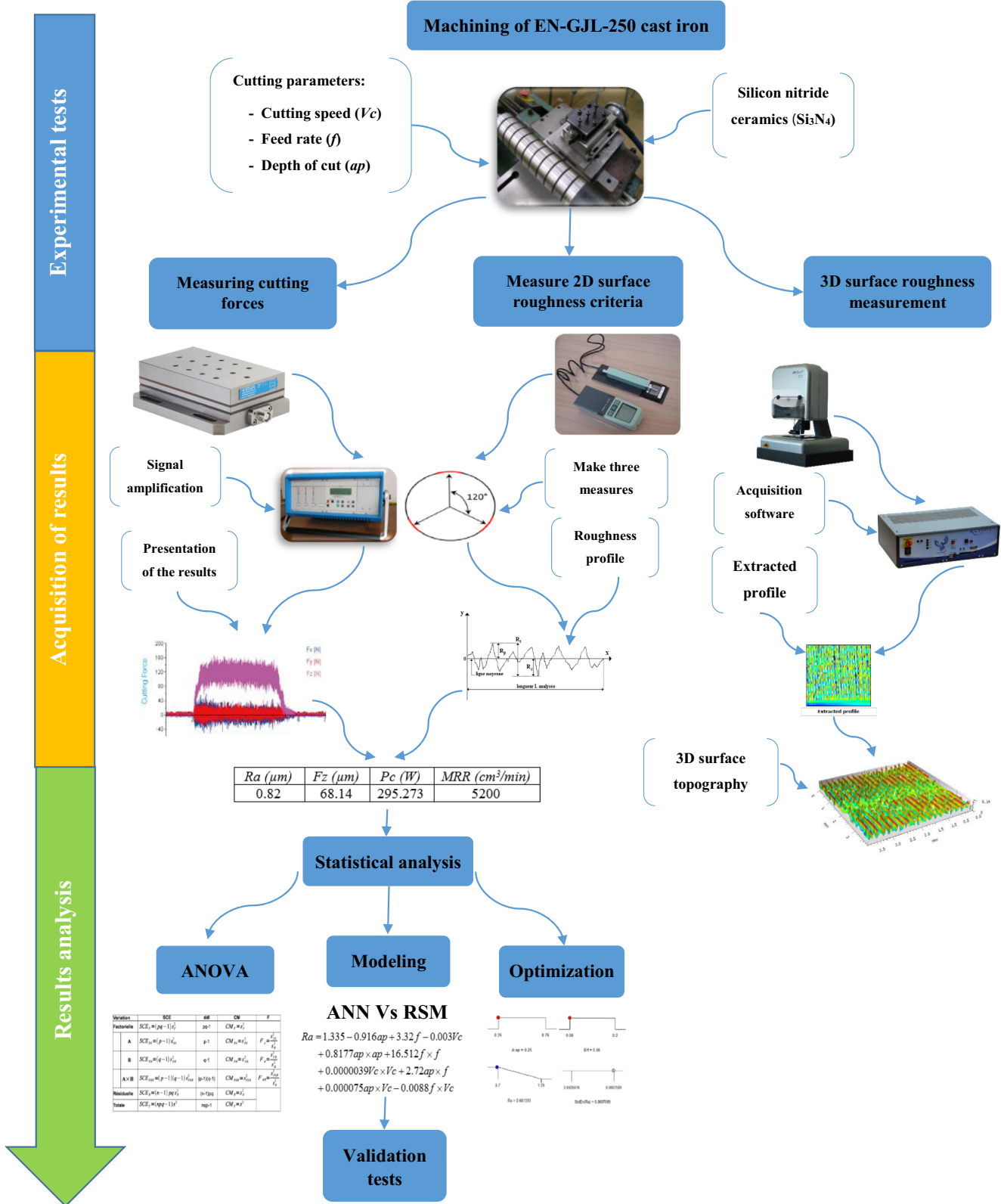


Fig. 1 Experimental setup

The cutting power P_c and the material removal rate (MRR) are expressed by the following two equations:

$$P_c = \frac{F_z \times V_c}{60} \quad (1)$$

Table 2 Levels of different cutting parameters

Levels	V_c (m/min)	f (mm/rev)	ap (mm)
1	260	0.08	0.25
2	370	0.14	0.5
3	530	0.2	0.75

$$MRR = ap \times V_c \times f \times 1000 \quad (2)$$

3.1 Statistical analysis

3.1.1 Analysis of variance (ANOVA)

The analysis of variance (ANOVA) is a statistical method applied to interpret the experimental results obtained. It classifies the various input parameters depending on their

influence on the technological parameters (outputs) [23, 24]. ANOVA's results for R_a , F_z , P_c , and MRR are represented in Tables 4, 5, 6, and 7, respectively. The analysis is performed for a significance level $\alpha = 0.05$ (i.e., for a 95% reliability level). A low probability value (≤ 0.05) indicates that the models obtained may be considered statistically significant [22] which is desirable.

Table 4 shows ANOVA's results for R_a for EN-GJL-250 cast iron obtained by the two Si_3N_4 ceramic tools coated (CC1690) and uncoated (CC6090). It may be noticed that the feed rate is found to be the most significant parameter with a contribution of 71.11% for CC6090 ceramic and 82.21% for CC1690. The cutting speed comes in second position with a contribution of 15.09% and 17.07% for CC6090 and CC1690, respectively. The cutting depth is identified to be the one having shown the weakest contribution with 3.53% and 3.32% for the two ceramics. The interaction ($f \times V_c$) for CC6090 and square terms (ap^2) and

Table 3 Results of R_a , F_z , MRR, and P_c according to the cutting conditions

No.	Input factors			Output factors							
				CC6090				CC1690			
	ap (mm)	f (mm/rev)	V_c (m/min)	R_a (μm)	F_z (N)	MRR (mm^3/min)	P_c (W)	R_a (μm)	F_z (N)	MRR (mm^3/min)	P_c (W)
1	0.25	0.08	260	0.82	68.14	5200	295.273	0.86	45.58	5200	197.513
2	0.25	0.08	370	0.77	54.90	7400	338.55	0.72	43.74	7400	269.73
3	0.25	0.08	530	0.72	57.73	10,600	509.948	0.64	30.73	10,600	271.448
4	0.25	0.14	260	1.29	100.86	9100	437.06	1.16	82.31	9100	356.677
5	0.25	0.14	370	0.91	78.67	12,950	485.132	0.91	75.23	12,950	463.918
6	0.25	0.14	530	0.83	75.84	18,550	669.92	0.83	61.88	18,550	546.607
7	0.25	0.2	260	1.53	111.96	13,000	485.16	1.86	107.14	13,000	464.273
8	0.25	0.2	370	1.39	96.95	18,500	597.858	1.76	82.06	18,500	506.037
9	0.25	0.2	530	1.18	93.79	26,500	828.478	1.66	76.58	26,500	676.457
10	0.5	0.08	260	0.75	127.92	10,400	554.32	0.55	115.93	10,400	502.363
11	0.5	0.08	370	0.73	93.33	14,800	575.535	0.52	90.07	14,800	555.432
12	0.5	0.08	530	0.7	99.16	21,200	875.913	0.45	84.48	21,200	746.24
13	0.5	0.14	260	1.35	202.69	18,200	878.323	0.88	153.68	18,200	665.94
14	0.5	0.14	370	0.88	195.14	25,900	1203.36	0.81	143.5	25,900	884.917
15	0.5	0.14	530	0.79	170.76	37,100	1508.38	0.77	133.8	37,100	1181.9
16	0.5	0.2	260	1.78	244.82	26,000	1060.89	1.65	206.42	26,000	894.487
17	0.5	0.2	370	1.43	230.98	37,000	1424.38	1.65	183.86	37,000	1133.8
18	0.5	0.2	530	1.27	219.40	53,000	1938.03	1.65	171.16	53,000	1511.91
19	0.75	0.08	260	0.93	193.54	15,600	838.673	0.62	151.26	15,600	655.46
20	0.75	0.08	370	0.85	192.04	22,200	1184.25	0.54	146.71	22,200	904.712
21	0.75	0.08	530	0.71	171.83	31,800	1517.83	0.47	137.73	31,800	1216.62
22	0.75	0.14	260	1.31	275.76	27,300	1194.96	0.87	246.17	27,300	1066.74
23	0.75	0.14	370	1.21	173.86	38,850	1688.8	0.8	239.2	38,850	1475.07
24	0.75	0.14	530	1.06	260.01	55,650	2296.76	0.77	221.69	55,650	1958.26
25	0.75	0.2	260	1.79	349.77	39,000	1515.67	1.53	307.2	39,000	1331.2
26	0.75	0.2	370	1.58	326.59	55,500	2013.97	1.5	255.12	55,500	1573.24
27	0.75	0.2	530	1.4	306.87	79,500	2710.68	1.43	173.4	79,500	1531.7

Table 4 ANOVA for R_a

Source	SC	DF	MC	F-value	Prob.	Cont.%	Remarks
a) CC6090							
Model	2.96	9	0.33	47	< 0.0001		Significant
$A: ap$ (mm)	0.11	1	0.11	15.56	0.001	3.53	Significant
$B: f$ (mm/rev)	2.19	1	2.19	312.88	< 0.0001	71.11	Significant
$C: V_c$ (m/min)	0.46	1	0.46	66.41	< 0.0001	15.09	Significant
$A \times B$	0.02	1	0.02	2.86	0.1089	0.65	Insignificant
$A \times C$	7.84E-05	1	7.84E-05	0.011	0.9168	0.0026	Insignificant
$B \times C$	0.062	1	0.062	8.85	0.0085	2.012	Significant
A^2	0.016	1	0.016	2.24	0.1525	0.509	Insignificant
B^2	0.021	1	0.021	3.03	0.0996	0.6897	Insignificant
C^2	0.028	1	0.028	4.06	0.0599	0.9235	Insignificant
Residual	0.12	17	6.98E-03				
Cor total	3.07	26					
b) CC1690							
Model	5.52	9	0.61	175.13	< 0.0001		Significant
$A: ap$ (mm)	0.19	1	0.19	53.05	< 0.0001	3.3296	Significant
$B: f$ (mm/rev)	4.81	1	4.81	1373.4	< 0.0001	86.2079	Significant
$C: V_c$ (m/min)	0.095	1	0.095	27.20	< 0.0001	17.072	Significant
AB	4.408E-03	1	4.048E-03	1.26	0.2777	0.0789	Insignificant
AC	0.012	1	0.012	3.51	0.0783	0.2203	Insignificant
BC	2.262E-03	1	2.262E-03	0.65	0.4329	0.0404	Insignificant
A^2	0.021	1	0.021	6.05	0.0249	0.3796	Significant
B^2	0.37	1	0.37	105.09	< 0.0001	6.5962	Significant
C^2	4.089E-03	1	4.089E-03	1.17	0.2952	0.0732	Insignificant
Residual	0.06	17	3.505E-03				
Cor total	5.58	26					

(f^2) for CC1690 ceramics are also observed to be significant with contributions of 2.012%, 0.37%, and 6.59%, respectively. No other interactions and square terms have been detected to be consequential. Their probabilities were greater than 0.05. Similar results have been encountered by other researchers [25, 26].

The results of ANOVA for (F_z) are presented in Table 5 and lead to the classification of the cutting regime (V_c , f , and ap) and their interactions concerning their influence on the tangential cutting force (F_z). The results obtained show that the depth of cut comes in first position with a contribution of 69.63% for CC6090 and 64.73% for CC1690. With the increase of ap , the thickness of the chip becomes important and leads to a volume growth of the metal deformed, thus requiring a significant cutting effort. The feed rate comes in second position with a contribution of 22.78% for CC6090 and 20.09% for CC1690, while the cutting speed is found to have an impact on F_z with a contribution of 1.3% for CC6090 and 4.28% for CC1690. The influence of ($ap \times f$) interaction is also found to be significant with a contribution of 3.74% for CC6090 and 1.45% for CC1690. The remaining parameters develop weak contributions of less than 1%. The results presented are found to be consistent with those of Nouioua et al. [8, 11].

Table 6 shows the ANOVA results for P_c . It can be seen that all the cutting parameters (i.e., V_c , f , and ap) along with all the interactions have an influence on the cutting power, the cutting depth developing the greatest impact with a contribution of 57.71% for CC690 and 61.87% for CC1690 ceramics. This is mainly due to the fact that the cutting power is straightly related to the tangential cutting force. It is directly followed by the feed rate with a contribution of (18.76 and 17.71)%, and the cutting speed that comes in third position with a contribution of (16.4 and 11.75)%.

The ANOVA's results concerning MRR for the two cutting materials tested are presented in Table 7. Based on these results, it may be concluded that both the three cutting regime parameters and their interactions have a significant effect on MRR. This result is expected, MRR being strictly related to the cutting depth, the cutting speed, and the feed rate (cf. Eq. 2). The impact of the three cutting regimes on MRR may be classified in terms of their influence. The cutting depth comes first with a contribution of 41.45% because the increase of ap leads to a similar increase in chip volume removed. It is followed by f with a contribution of 30.45%, and this may

Table 5 ANOVA for F_z

Source	SC	DF	MC	<i>F</i> -value	Prob.	Cont.%	Remarks
a) CC6090							
Model	203,184.1	9	22,576.01	182.664	<0.0001		Significant
<i>A</i> : <i>ap</i> (mm)	142,940.1	1	142,940.1	1156.54	<0.0001	69.63	Significant
<i>B</i> : <i>f</i> (mm/rev)	46,766.25	1	46,766.25	378.390	<0.0001	22.78	Significant
<i>C</i> : <i>Vc</i> (m/min)	2690.600	1	2690.600	21.7698	0.0002	1.310	Significant
<i>A</i> × <i>B</i>	7695.761	1	7695.761	62.2671	<0.0001	3.748	Significant
<i>A</i> × <i>C</i>	81.01512	1	81.01512	0.65550	0.4293	0.039	Insignificant
<i>B</i> × <i>C</i>	59.43121	1	59.43121	0.48086	0.4973	0.028	Insignificant
<i>A</i> ²	116.4241	1	116.4241	0.94199	0.3453	0.056	Insignificant
<i>B</i> ²	958.1120	1	958.1120	7.75217	0.0127	0.466	Significant
<i>C</i> ²	137.5766	1	137.5766	1.11314	0.3061	0.067	Insignificant
Residual	2101.076	17	123.5927				
Cor total	205,285.1	26					
b) CC1690							
Model	130,875.5	9	14,541.72	46.55	<0.0001		Significant
<i>A</i> : <i>ap</i> (mm)	88,159.44	1	88,159.44	282.2	<0.0001	64.73	Significant
<i>B</i> : <i>f</i> (mm/rev)	27,370.58	1	27,370.58	87.63	<0.0001	20.09	Significant
<i>C</i> : <i>Vc</i> (m/min)	5840.643	1	5840.643	18.69	0.0005	4.288	Significant
AB	1983.783	1	1983.783	6.351	0.0220	1.456	Significant
AC	976.3272	1	976.3272	3.125	0.0950	0.716	Insignificant
BC	1616.936	1	1616.936	5.176	0.0361	1.187	Significant
<i>A</i> ²	124.7312	1	124.7312	0.399	0.5358	0.091	Insignificant
<i>B</i> ²	1731.167	1	1731.167	5.542	0.0308	1.271	Significant
<i>C</i> ²	42.54456	1	42.54456	0.136	0.1362	0.031	Insignificant
Residual	5309.746	17	312.3380				
Cor total	136,185.2	26					

be interpreted as a result of the increase of the chip section. In third position comes the cutting speed with a contribution of 19.48%. The three interactions are also found to be significant with contributions of 4.89%, 3.28%, and 2.41% for (*ap* × *Vc*), (*ap* × *f*), and (*Vc* × *f*), respectively. The influence of the three square terms is identified to be insignificant.

3.1.2 Graphical representations of principal effects

Figure 2a–h represents the evolution of *Ra*, *Fz*, *Pc*, and MRR as a function of the input parameters (*ap*, *f*, and *Vc*). They confirm the ANOVA results illustrated in Tables 4, 5, 6, and 7. It can be seen that concerning *Ra* obtained for the two ceramics (CC6090 and CC1690), *f* displays the greatest gradient indicating its great influence, the tool movement relatively to the part generating helical grooves in turning processes. These grooves are found to be deeper and wider as the feed is higher [27]. It should be mentioned that *Ra* decreases with the increase of *Vc* as a result of the elevation of the temperature in the cutting zone that leads to the machined metal becoming more plastic, consequently decreasing both the

necessary force in cutting and the roughness criteria. Inversely, the cutting depth displays the smallest gradient indicating a very low effect on the surface roughness. Moreover, an increase of *Fz* results in a similar increase of *ap* that prompts a rise of the volume of the removed metal along with the cross section of the chip which is a consequence of the augmentation of *f*, the cutting forces required becoming more significant [28]. Furthermore, the increase of *Vc* generates a decrease of *Fz*. Finally and as far as MRR and *Pc* are concerned, their increase is found to follow that of the three cutting parameters.

4 Modeling of cutting parameters

4.1 Response surface methodology model

The response surface methodology is a combination of mathematical and statistical techniques used to develop a mathematical model for both analysis and optimization. In the present case, it is used to model a dependent variable noted (\bar{Y})

Table 6 ANOVA for P_c

Source	SC	DF	MC	F-value	Prob.	Cont.%	Remarks
a) CC6090							
Model	10,460,715.9	9	1,162,301.77	164.53	<0.0001		Significant
A: ap (mm)	6,106,591.49	1	6,106,591.49	864.43	<0.0001	57.713	Significant
B: f (mm/rev)	1,985,508.52	1	1,985,508.52	281.06	<0.0001	18.765	Significant
C: V_c (m/min)	1,739,496.92	1	1,739,496.92	246.24	<0.0001	16.440	Significant
$A \times B$	311,003.702	1	311,003.702	44.025	<0.0001	2.9393	Significant
$A \times C$	391,571.442	1	391,571.442	55.430	<0.0001	3.7007	Significant
$B \times C$	119,525.056	1	119,525.056	16.919	0.0007	1.1296	Significant
A^2	3412.72300	1	3412.72300	0.4830	0.4964	0.0322	Insignificant
B^2	39,473.0827	1	39,473.0827	5.5877	0.0302	0.3730	Significant
C^2	58.1845688	1	58.1845688	0.0082	0.9287	0.0005	Insignificant
Residual	120,091.937	17	7064.23161				
Cor total	10,580,807	26					
b) CC1690							
Model	5,497,357.12	9	610,817.457	33.142	<0.0001		Significant
A: ap (mm)	3,595,114.61	1	3,595,114.61	195.07	<0.0001	61.87	Significant
B: f (mm/rev)	1,029,355.63	1	1,029,355.63	55.852	<0.0001	17.71	Significant
C: V_c (m/min)	683,079.836	1	683,079.836	37.063	<0.0001	11.75	Significant
AB	47,034.9278	1	47,034.9278	2.5521	0.1285	0.809	Insignificant
AC	112,023.743	1	112,023.743	6.0784	0.0246	1.927	Significant
BC	1664.37491	1	1664.37491	0.0903	0.7674	0.028	Significant
A^2	8774.59291	1	8774.59291	0.4761	0.4995	0.151	Insignificant
B^2	94,370.7464	1	94,370.7464	5.1205	0.0370	1.624	Significant
C^2	3036.79163	1	3036.79163	0.1647	0.6898	0.052	Insignificant
Residual	313,305.997	17	18,429.7645				
Cor total	5,810,663.11	26					

Table 7 ANOVA for MRR

Source	SC	DF	MC	F-value	Prob.	Cont.%	Remarks
a) CC6090							
Model	8.218E09	9	9.131E08	467.86	<0.0001		Significant
A: ap (mm)	3.421E09	1	3.421E09	1752.78	<0.0001	41.459	Significant
B: f (mm/rev)	2.513E09	1	2.513E09	1287.76	<0.0001	30.459	Significant
C: V_c (m/min)	1.607E09	1	1.607E09	823.59	<0.0001	19.480	Significant
$A \times B$	4.037E08	1	4.037E08	206.83	<0.0001	4.8921	Significant
$A \times C$	2.710E08	1	2.710E08	138.83	<0.0001	3.2838	Significant
$B \times C$	1.991E08	1	1.991E08	102	<0.0001	2.4126	Significant
A^2	0	1	0	0	1	0	Insignificant
B^2	0	1	0	0	1	0	Insignificant
C^2	0	1	0	0	1	0	Insignificant
Residual	3.318E07	17	1.952E06				
Cor total	8.252E09	26					

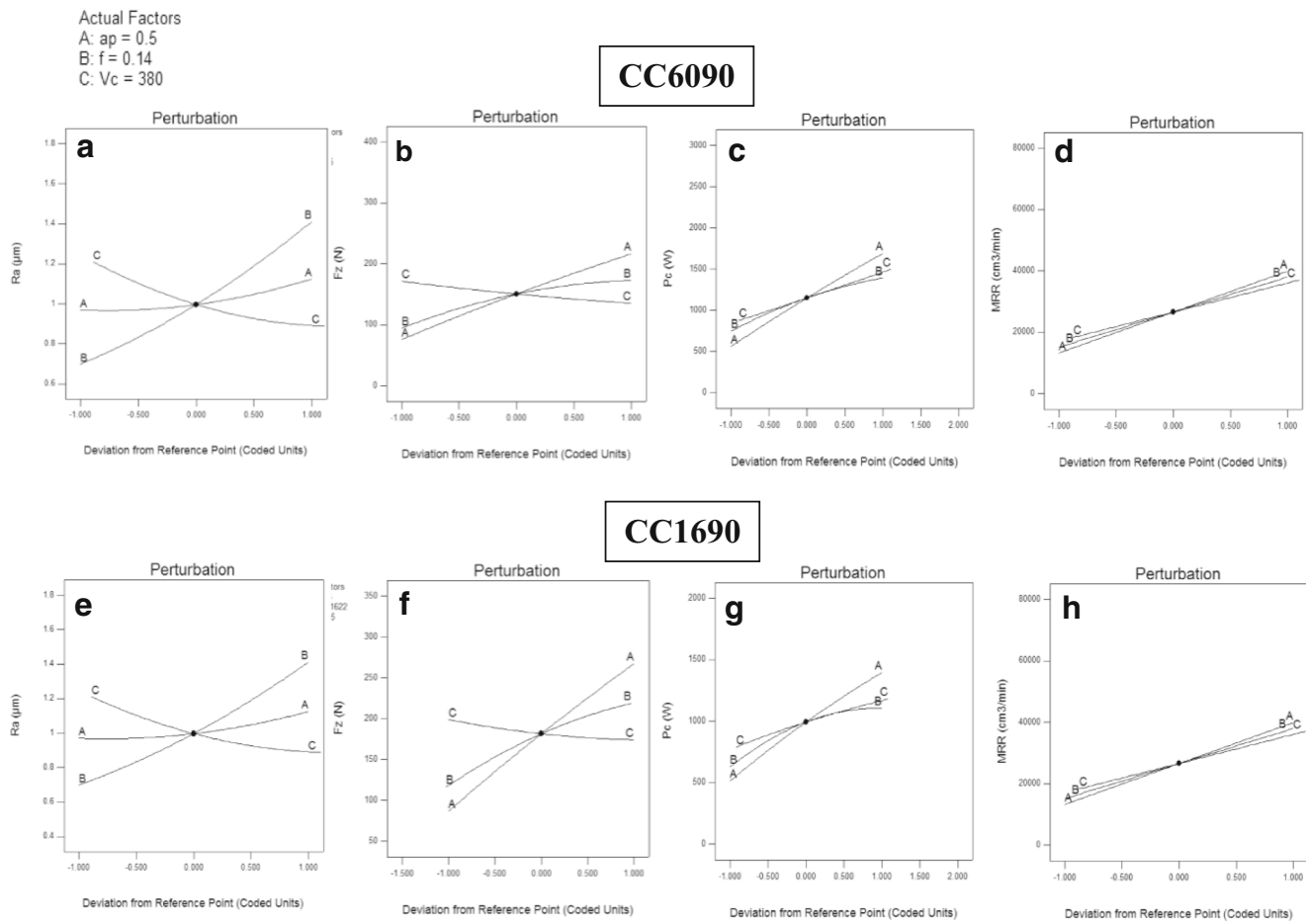


Fig. 2 Main affects graphs for R_a , F_z , P_c , and MRR

and called response variable (represented by the surface roughness and the cutting force) as a function of a number of independent variables noted X_1, X_2, \dots, X_k [29].

The model used in this study is a quadratic polynomial integrating interactions in the form:

$$\bar{Y} = a_0 + \sum_{i=1}^k a_i X_i + \sum_{i=1}^k a_{ii} X_i^2 + \sum_{i < j} a_{ij} X_i X_j \quad (3)$$

\bar{Y} is the parameter of interest to the experimenter and represents the response or the parameter of interest. It is measured during the experiment and obtained to a given precision.

Fig. 3 Graphical representation of an ANN

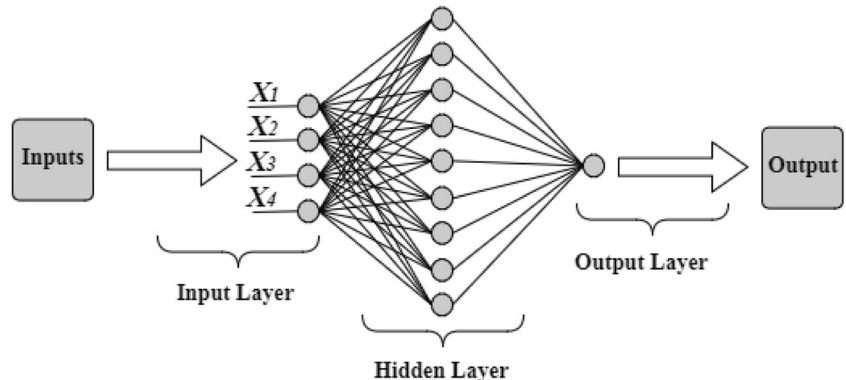


Table 8 ANN appropriate architecture for modeling Ra , F_z , and P_c

	Appropriate architecture	
	CC6090	CC1690
Ra	3-12-1	3-4-1
F_z	3-3-1	3-5-1
P_c	3-4-1	3-3-1

a_0 , a_i , and a_{ii} are the constants in Eq. (3). They represent respectively the constant term, the linear term coefficients, and the quadratic term coefficients. They are unknowns and hence should be determined from the experimental results. The regression analysis of Ra , F_z , and P_c according to the cutting regime is described by the equations of the complete model (i.e., 4 to 9).

(X_i) is the level allocated to factor (i) and represents its perfectly known coordinate that would be retained by the experimenter in order to realize a test.

$$Ra_{CC6090} = 1.335 - 0.916ap + 3.32f - 0.003Vc + 0.8177ap \times ap + 16.512f \times f + 0.0000039Vc \times Vc + 2.72ap \times f + 0.000075ap \times Vc - 0.0088f \times Vc \quad (4)$$

$$Ra_{CC1690} = 2.02 - 1.55ap - 10.65f - 2.42 \times 10^{-3}Vc + 0.95ap^2 + 68.827f^2 + 1.49 \times 10^{-6}Vc^2 - 1.27ap \times f + 9.43 \times 10^{-4}ap \times Vc + 1.68 \times 10^{-3}f \times Vc \quad (5)$$

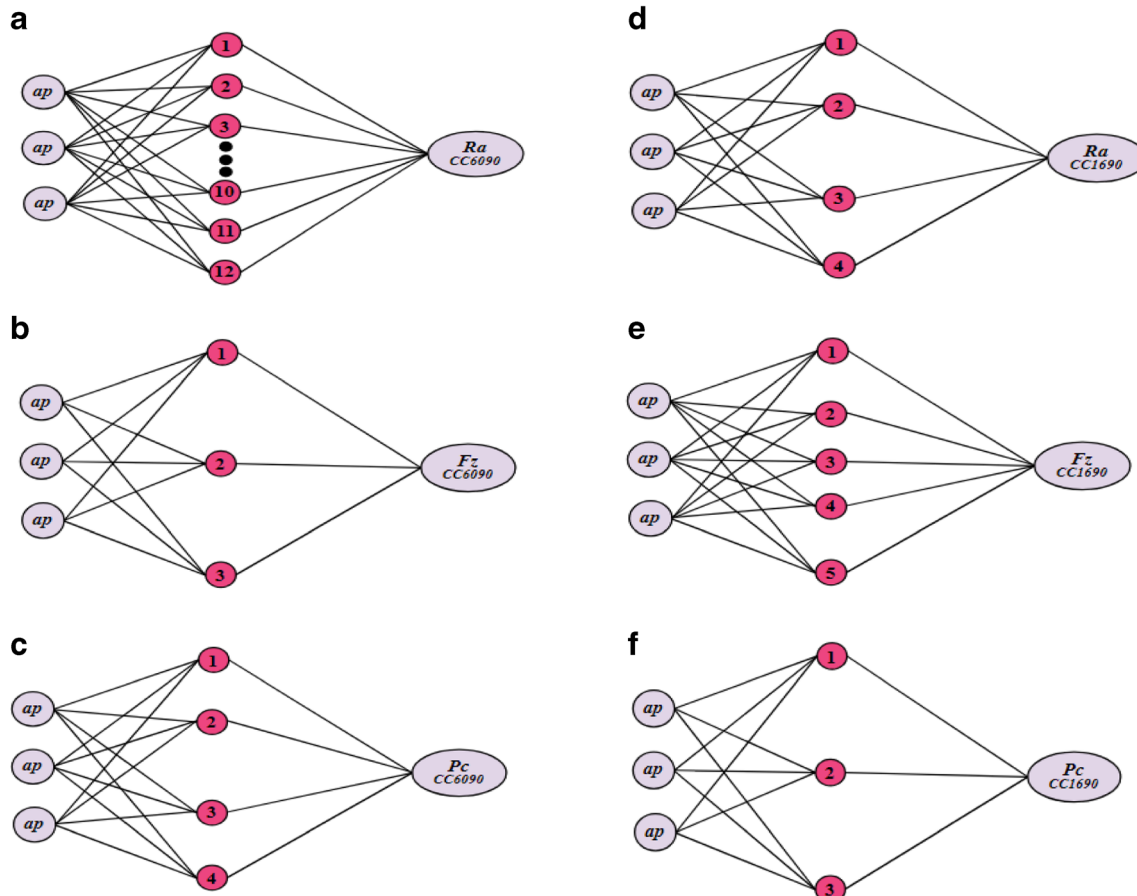


Fig. 4 ANN perceptrons for Ra , F_z , and P_c

$$Fz_{CC6090} = -37.689 + 221.81ap + 1098.54f - 0.2302Vc - 70.48ap \times f - 3510.18f \times f + 0.00027Vc \times Vc + 1688.27ap \times f - 0.0765ap \times Vc - 0.273f \times Vc \quad (6)$$

$$Fz_{CC1690} = -186.28 + 338.64ap + 2107.16f + 0.0787Vc - 72.951ap \times f - 4718.36f \times f + 0.00015Vc \times Vc + 857.16ap \times f - 265ap \times Vc - 1.424f \times Vc \quad (7)$$

$$Pc_{CC6090} = 300.019 - 886.74ap + 1654.02f - 2.21Vc - 381.58ap \times f - 22530.58f \times f + 0.00017Vc \times Vc + 10732.5ap \times f + 5.32ap \times Vc + 12.25f \times Vc \quad (8)$$

$$Pc_{CC1690} = -1118.96 + 695.82ap + 11093.27f + 0.83Vc - 611.86ap \times f - 34836.98f \times f - 0.00128Vc \times Vc + 4173.76ap \times f + 2.84ap \times Vc + 1.44f \times Vc \quad (9)$$

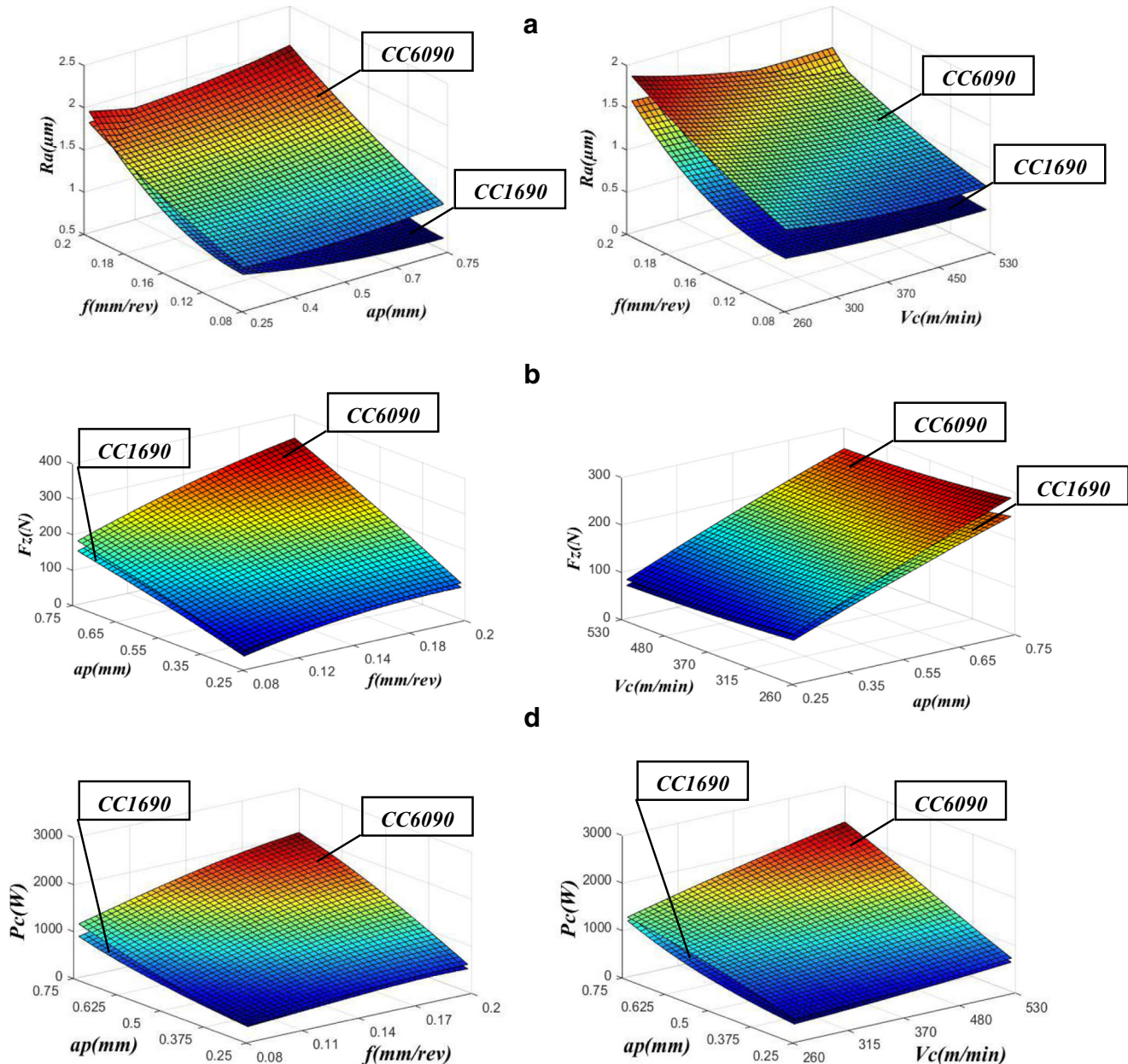


Fig. 5 3D response surfaces for R_a , F_z , and P_c

4.2 Artificial neural networks model

Artificial neural networks are one of the methods of artificial intelligence that was inspired from the behavior of the human brain in order to perform useful functions pertaining to industrial applications such as the assignment of approximation, classification, and modeling tasks. It uses a non-linear and bounded algebraic function whose value depends on parameters called coefficients (weight). An ANN model consists of three connected layers constituted each of one or more neurons. The first layer is the input in which each neuron represents a variable, while the second layer is the hidden layer. This latter receives the information from the input layer and processes it using a transfer function. Finally, the last layer is the output layer that can be constituted of one or more outputs which represent the numerical values of the responses or dependent variables [30]. An ANN model is usually represented graphically as shown in Fig. 3.

The most frequently used neurons are those for which the transfer function (f) is a non-linear function (usually a hyperbolic tangent) of a linear combination of the inputs:

$$f = \tanh \sum_{i=1}^n w_i x_i \quad (10)$$

where (x_i) represent the neuron input variables, (w_i) the adjustable parameters, and (n) the neuron number.

In order to model the R_a , F_z , and P_c criteria, six multi-layer perceptrons (constituted of one input, one hidden, and one output layer) were used. Each perceptron had one output only because ANN models with single outputs give better results compared to those with several outputs [1]. The experimental procedure consisted of 27 trials of which 18 tests were used for network learning and 9 validation tests randomly selected to assess the effectiveness of the network. The learning of the neural network was performed through the application of a retro-propagation algorithm based on a descending gradient. In the present case, a learning rate of $\eta = 0.1$ was selected.

Table 8 and Fig. 4 present the adequate ANN architectures to model the R_a , F_z , and P_c criteria for the two tested ceramics investigated.

Table 9 Comparison between RSM and ANN prediction results for CC6090

No.	Predicted surface roughness (R_a)		Absolute prediction error (%)		Predicted cutting force (F_z)		Absolute prediction error (%)		Predicted cutting power (P_c)		Absolute prediction error (%)	
	RSM	ANN	RSM	ANN	RSM	ANN	RSM	ANN	RSM	ANN	RSM	ANN
1	0.86	0.83	5.46	1.64	60.5293	67.4871	11.1691	0.95809	294.396	270.741	0.29680	8.30811
2	0.72	0.76	6.38	0.70	49.6597	60.2601	9.54500	9.76350	317.351	308.931	6.26166	8.74856
3	0.68	0.71	5.37	1.28	45.6700	51.7100	20.8903	10.4278	358.426	518.858	29.7132	1.74724
4	1.19	1.25	8.11	3.25	101.170	93.4031	0.30768	7.39331	448.343	461.010	2.58175	5.47981
5	0.98	0.93	8.05	2.30	88.4977	85.6598	12.4923	8.88506	552.157	521.669	13.8159	7.53148
6	0.86	0.84	3.51	0.97	81.8852	76.3153	7.97111	0.62673	710.845	704.568	6.10905	5.17204
7	1.62	1.55	6.20	1.56	116.537	112.428	4.08892	0.41827	440.070	446.566	9.29373	7.95470
8	1.36	1.38	1.83	0.82	102.062	105.024	5.27311	8.32883	624.743	587.972	4.49685	1.65349
9	1.16	1.20	2.05	1.44	92.8272	95.8299	1.02648	2.17498	901.045	817.871	8.75904	1.28022
10	0.85	0.74	13.09	1.28	131.558	126.498	2.84412	1.11096	561.741	530.068	1.33884	4.37494
11	0.71	0.72	3.24	2.04	118.583	114.961	27.0582	23.1772	731.050	643.878	27.0209	11.8747
12	0.67	0.71	4.30	0.92	111.531	99.1730	12.4764	0.01313	985.004	896.501	12.4545	2.35043
13	1.21	1.30	10.40	3.76	197.523	204.912	2.54904	1.09670	876.675	915.738	0.18756	4.25984
14	1.01	0.92	14.73	4.00	182.745	191.052	6.35156	2.09462	1126.84	1136.70	6.35881	5.53943
15	0.89	0.76	12.47	3.84	173.071	172.617	1.35342	1.08771	1498.41	1468.78	0.66089	2.62488
16	1.69	1.72	5.06	3.58	238.215	245.810	2.69784	0.40463	1029.39	1069.88	2.96889	0.84811
17	1.43	1.41	0.12	1.22	221.634	232.632	4.04610	0.71526	1360.41	1421.99	4.49035	0.16714
18	1.23	1.25	3.46	1.65	209.337	215.537	4.58649	1.76063	1849.59	1883.92	4.56314	2.79203
19	0.93	0.91	0.42	2.67	193.777	193.440	0.12247	0.05148	781.387	862.980	6.83052	2.89828
20	0.79	0.84	6.57	1.35	178.697	185.427	6.94794	3.44343	1097.05	1136.97	7.36301	3.99205
21	0.76	0.71	7.13	0.50	168.583	172.156	1.88948	0.18993	1563.88	1526.94	3.03406	0.60069
22	1.34	1.35	2.00	3.22	285.066	283.023	3.37479	2.63411	1257.30	1256.57	5.21769	5.15610
23	1.14	1.21	5.93	0.15	268.183	273.851	2.07280	0.00315	1653.83	1684.46	2.07080	0.25702
24	1.02	1.00	3.76	5.89	255.446	259.355	1.75496	0.25190	2238.27	2230.32	2.54606	2.89229
25	1.86	1.82	3.76	1.65	351.082	339.116	0.37518	3.04593	1571.01	1499.72	3.65126	1.05232
26	1.60	1.57	1.34	0.59	332.396	326.159	1.77786	0.13176	2048.39	2052.67	1.70909	1.92156
27	1.39	1.40	0.11	0.52	317.037	307.735	3.31320	0.28199	2750.45	2742.15	1.46706	1.16113

The mathematical models obtained by the ANN method for the three criteria Ra , Fz , and Pc for the two cutting tools (CC1690 and CC6090) are expressed by the following equations:

$$\begin{aligned} Ra_{CC6090} = & 0.20H_1 - 0.46H^2 - 0.38H_3 + 0.39H_4 - 0.32H_5 + 0.16H_6 \\ & - 0.09H_7 - 0.14H_8 - 0.30H_9 - 0.32H_{10} + 0.50H_{11} + 0.31H_{12} + 1.54 \end{aligned} \quad (11)$$

with:

$$\begin{aligned} H_1 &= \text{Tanh}(0.5(3.21ap - 33.73f - 0.016Vc + 9.13)) \\ H_2 &= \text{Tanh}(0.5(7.22ap + 37.12f - 0.009Vc - 4.94)) \\ H_3 &= \text{Tanh}(0.5(3.07ap - 23.89f - 0.003Vc + 3.13)) \\ H_4 &= \text{Tanh}(0.5(-5.13ap - 16.07f + 0.01Vc - 0.78)) \\ H_5 &= \text{Tanh}(0.5(8.48ap + 26.54f - 0.003Vc - 5.58)) \\ H_6 &= \text{Tanh}(0.5(1.84ap - 17.20f - 0.004Vc + 3.01)) \\ H_7 &= \text{Tanh}(0.5(-0.34ap + 15.73f + 0.008Vc - 7.72)) \\ H_8 &= \text{Tanh}(0.5(3.12ap + 0.49f - 0.004Vc - 2.90)) \\ H_9 &= \text{Tanh}(0.5(-7.38ap - 1.73f + 0.009Vc + 0.37)) \\ H_{10} &= \text{Tanh}(0.5(-2.74ap - 20.16f - 0.003Vc + 6.44)) \\ H_{11} &= \text{Tanh}(0.5(-2.55ap - 23.43f - 0.009Vc + 0.81)) \\ H_{12} &= \text{Tanh}(0.5(4.59ap - 14.08f + 0.01Vc - 5.02)) \end{aligned}$$

$$\begin{aligned} Ra_{CC1690} = & -9.97H_1 + 16.61H^2 - 6.35H_3 + 3.86H_4 \\ & + 6.62 \end{aligned} \quad (12)$$

with:

$$\begin{aligned} H_1 &= \text{Tanh}(0.5(-128ap - 7.27f - 0.00074Vc + 2.24)) \\ H_2 &= \text{Tanh}(0.5(-0.076ap - 6.701f - 0.00067Vc - 1.02)) \\ H_3 &= \text{Tanh}(0.5(0.96ap - 7.998f + 0.0092Vc + 1.048)) \\ H_4 &= \text{Tanh}(0.5(-1.74ap + 3.69f + 0.0021Vc - 0.565)) \end{aligned}$$

$$Fz_{CC6090} = 112.06H_1 - 198.43H^2 - 233.97H_3 + 113.49 \quad (13)$$

with:

$$\begin{aligned} H_1 &= \text{Tanh}(0.5(7.94ap + 11.07f - 0.0006Vc - 5.20)) \\ H_2 &= \text{Tanh}(0.5(-4.46ap + 8.90f + 0.0018Vc + 1.29)) \\ H_3 &= \text{Tanh}(0.5(4.83ap - 17.49f - 0.001Vc - 1.33)) \end{aligned}$$

$$\begin{aligned} Fz_{CC1690} = & 103.61H_1 - 71.85H^2 - 107.64H_3 - 52.75H_4 \\ & - 90.45H_5 + 31.06 \end{aligned} \quad (14)$$

Table 10 Comparison between RSM and ANN prediction results for CC1690

No.	Predicted surface roughness (Ra)		Absolute prediction error (%)		Predicted cutting force (Fz)		Absolute prediction error (%)		Predicted cutting power (Pc)		Absolute prediction error (%)	
	RSM	ANN	RSM	ANN	RSM	ANN	RSM	ANN	RSM	ANN	RSM	ANN
1	0.82	0.87	4.54	1.51	33.1773	48.8039	27.2107	7.07313	109.482	222.090	44.5693	12.4431
2	0.70	0.75	3.01	4.84	32.5345	45.7309	25.6183	4.55185	203.015	292.103	24.7336	8.29488
3	0.58	0.61	8.69	4.94	38.1728	26.3160	24.2200	14.3635	283.528	261.593	4.45013	3.63051
4	1.10	1.11	5.41	4.40	87.9528	80.5735	6.85565	2.10962	400.390	342.973	12.2559	3.84186
5	0.99	1.00	8.33	9.44	77.9053	76.0692	3.55618	1.11559	503.465	438.240	8.52459	5.53499
6	0.89	0.84	6.99	1.29	69.8640	53.5560	12.9024	13.4517	597.856	617.989	9.37601	13.0592
7	1.87	1.83	0.49	1.45	108.756	100.318	1.50848	6.36728	440.472	362.615	5.12646	21.8960
8	1.77	1.77	0.50	0.44	89.3038	91.8595	8.82755	11.9418	553.088	492.468	9.29816	2.68132
9	1.69	1.66	1.64	0.26	67.5829	79.8320	11.7485	4.24658	661.358	768.055	2.23191	13.5409
10	0.65	0.57	17.61	3.35	104.029	90.6641	10.2651	21.7940	437.217	393.661	12.9679	21.6380
11	0.55	0.50	5.81	3.96	96.0787	87.3677	6.67119	3.00012	609.031	499.916	9.65003	9.99494
12	0.47	0.46	5.34	2.59	91.0872	73.1331	7.82107	13.4314	803.406	698.412	7.66057	6.40907
13	0.90	0.88	2.74	0.19	171.662	160.084	11.7013	4.16753	790.731	614.316	18.7380	7.75295
14	0.82	0.82	1.05	0.81	154.307	160.234	7.53103	11.6614	972.087	794.114	9.85070	10.2610
15	0.76	0.77	1.49	0.30	135.635	139.181	1.37214	4.02240	1180.34	1151.41	0.13188	2.57966
16	1.66	1.67	0.41	1.29	205.323	203.551	0.53124	1.38951	893.419	862.754	0.1192	3.54747
17	1.58	1.64	4.10	0.89	178.563	188.777	2.88093	2.67439	1084.31	1105.46	4.36463	2.49948
18	1.54	1.60	6.75	3.08	146.212	155.821	14.5756	8.96133	1306.44	1383.41	13.5896	8.49876
19	0.59	0.60	4.56	3.94	165.762	146.720	9.58804	3.00096	688.468	678.789	5.03588	3.55923
20	0.52	0.53	3.52	1.16	150.504	145.904	2.58610	0.54908	938.562	869.864	3.74163	3.85174
21	0.48	0.53	2.67	12.63	134.882	143.002	2.06725	3.82789	1246.80	1248.14	2.48113	2.59194
22	0.83	0.86	4.63	0.62	246.253	249.871	0.03388	1.50363	1104.58	1178.26	3.54843	10.4551
23	0.77	0.80	3.73	0.49	221.589	243.192	7.36209	1.66900	1364.22	1479.41	7.51432	0.29471
24	0.75	0.77	2.87	0.29	192.288	211.095	13.2622	4.77877	1686.34	1852.15	13.8857	5.41866
25	1.56	1.54	2.18	0.79	292.771	284.397	4.69670	7.42268	1269.88	1490.11	4.60608	11.9374
26	1.51	1.48	0.99	1.15	258.703	251.324	1.40460	1.48780	1539.06	1588.27	2.17247	0.95555
27	1.51	1.45	5.51	1.35	215.722	190.227	24.4076	9.70453	1875.05	1610.82	22.4167	5.16599

Table 11 Error functions and its equations

Error function	Equation
Mean absolute deviation	$MAD = \sum_{t=1}^n \frac{ E_t - P_t }{n}$ (15)
Mean absolute percentage error (%)	$MAPE = \sum_{t=1}^n \frac{ (E_t - P_t)/E_t }{n} \times 100$ (16)
Root mean square error	$RMSE = \sqrt{\frac{\sum_{t=1}^n (P_t - E_t)^2}{n}}$ (17)
Correlation coefficient	$R^2 = \frac{\sum_{t=1}^n (P_t - E_t)(Y_t - \bar{Y}_e)}{\sum_{t=1}^n (P_t - E_t)^2}$ (18)

n number of experiments, E_t experimental value of the t th experiment, P_t predicted value of the t th experiment by model, \bar{Y}_e average of the experimentally determined values

with:

$$\begin{aligned} H_1 &= \text{Tanh}(0.5(2.78ap + 3.26f + 0.0013Vc - 1.56)) \\ H_2 &= \text{Tanh}(0.5(3.20ap - 6.58f + 0.006Vc - 4.38)) \\ H_3 &= \text{Tanh}(0.5(-1.49ap + 27.78f + 0.0049Vc - 6.24)) \\ H_4 &= \text{Tanh}(0.5(-769ap - 20.89f - 0.0038Vc + 8.87)) \\ H_5 &= \text{Tanh}(0.5(-1.94ap - 29.85f - 0.003Vc + 6.13)) \\ P_{CC6090} &= 3380.41H_1 - 3624.74H_2^2 - 14873.51H_3 - 6461.44H_4 \quad (15) \\ &\quad + 1510.29 \end{aligned}$$

with:

$$\begin{aligned} H_1 &= \text{Tanh}(0.5(2.24ap + 5.51f + 0.0024Vc - 3.85)) \\ H_2 &= \text{Tanh}(0.5(1.09ap - 10.27f - 0.0001Vc - 0.26)) \\ H_3 &= \text{Tanh}(0.5(0.42ap + 5.39f - 0.0008Vc - 0.45)) \\ H_4 &= \text{Tanh}(0.5(-1.81ap - 7.66f + 0.0024Vc + 0.63)) \\ P_{CC1690} &= -831.51H_1 - 665.87H_2^2 - 658.41H_3 - 455.92 \quad (16) \end{aligned}$$

with:

$$\begin{aligned} H_1 &= \text{Tanh}(0.5(1.40ap + 35.41f + 0.0023Vc - 9.59)) \\ H_2 &= \text{Tanh}(0.5(-7.44ap - 31.56f - 0.0065Vc + 12.22)) \\ H_3 &= \text{Tanh}(0.5(-2.54ap - 9.62f - 0.0027Vc + 3.51)) \end{aligned}$$

4.3 3D response surfaces

Figure 5a–c shows the 3D response surfaces for R_a , F_z , and P_c as a function of V_c , f , and ap for the two ceramics tested. The results exhibit a considerable increase in R_a with the augmentation of the feed rate and that they are not statistically influenced by the variation of the cutting depth. Feng et al. [31] reported similar results, acknowledging that the depth of cut does not affect the surface roughness and that the increase in cutting speed leads to a reduction of R_a . Moreover, the increase of ap and f leads to a sharp rise of F_z , while the augmentation of V_c decreases it. It is also found that the coated ceramic tool (CC1690) leads to a better surface roughness and needs less cutting forces than those obtained by the uncoated ceramics (CC6090).

4.4 Comparison between ANN and RSM models

Tables 9 and 10 show the results of R_a , F_z , and P_c predicted by both the RSM and ANN models for the two ceramics (CC6090 and CC1690) along with the percentages of their absolute prediction errors. It can be seen that the ANN models provide better results with low errors compared to those produced by the RSM models. For the CC6090 cutting insert, the maximum RSM values of the absolute error for R_a , F_z , and P_c criteria are found equal to (14.73, 27.05, and 29.71)% respectively, while for the ANN models, they correspond to (5.89, 23.17, and 11.87)% For the second cutting insert (CC1690), the maximum errors of RSM are (17.61, 27.21, and 44.56)% while those for ANN are (12.63, 21.79, and 21.89)%.

In order to properly evaluate the predictive capabilities of the models developed by the two approaches, the experimental and predicted results are compared in terms of the mean square error (MSE), mean root square error (RMSE), mean absolute error (MAD), absolute mean percentage error (MAPE), and coefficient of determination (R^2). The relationships expressing the different error criteria are presented in Table 11.

Table 12 presents the values of MAD, MAPE, RMSE, and R^2 obtained from the application of the response surface

Table 12 Comparison between ANN and RSM

	CC6090						CC1690					
	R_a		F_z		P_c		R_a		F_z		P_c	
	RSM	ANN	RSM	ANN	RSM	ANN	RSM	ANN	RSM	ANN	RSM	ANN
MAD	0.054	0.021	7.13	3.78	53.97	31.06	0.037	0.02	10.380	7.544	73.6	61.11
MAPE (%)	5.36	1.955	5.86	3.35	6.49	3.80	2.28	2.49	9.303	6.306	9.74	7.49
RMSE	0.012	0.001	1.69	0.22	12.83	1.35	0.009	0.001	2.96	0.36	20.73	2.78
R^2	0.96	0.99	0.98	0.99	0.98	0.99	0.98	0.99	0.96	0.99	0.94	0.96

methodology (RSM) and the artificial neural network approach (ANN) for R_a , F_z , and P_c concerning the two ceramics tested (CC6090 and CC1690). The results obtained show clearly that the models derived from the neural network method (ANN) give better results than those obtained from the response surface methodology (RSM). The values predicted by RSM and ANN methods were in the limits of $\pm 9\%$ and $\pm 7\%$, respectively. On the other hand, the MAD predicted by the ANN does not

exceed 61.11, while it reaches 73.6 for the RSM models. Concerning the RSME, the ANN models predict lower values (between 0.001 and 2.78) than that given by the RSM models (between 0.009 and 20.73). Finally, it should be pointed out that all models obtained by the ANN approach have a coefficient of determination (R^2) very close to unity ($R^2 = 0.99$) except for (P_c) where it is found equal to ($R^2 = 0.96$). The (R^2) of the models obtained by RSM vary between 0.94 and 0.98.

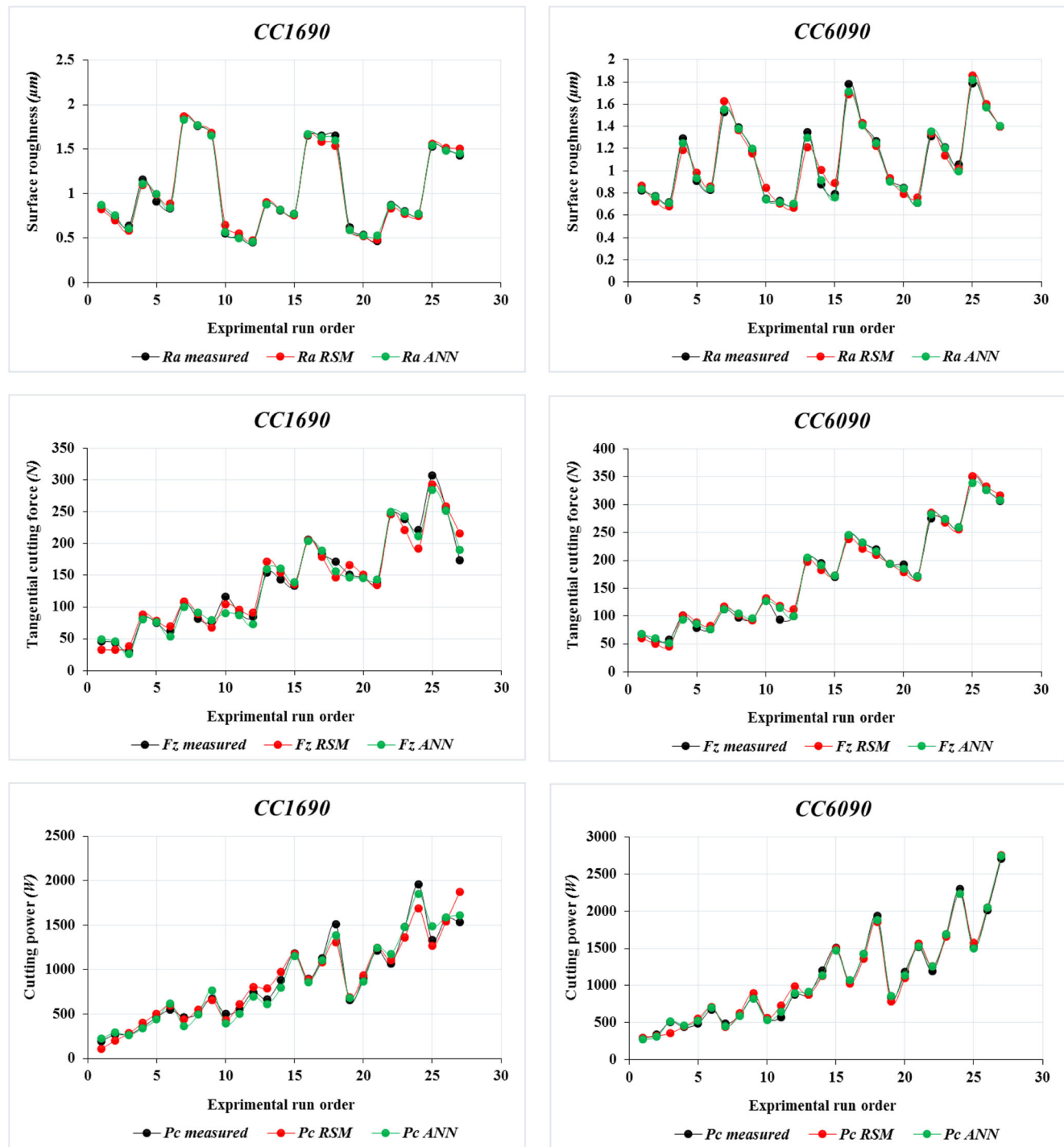


Fig. 6 Comparison between experimental values and estimates by RSM and ANN

The comparison between the experimental values (measured) of Ra , F_z , and P_c , and those estimated by the mathematical models obtained by the RSM and ANN methods is presented in Fig. 6. They are found very close. However, the models obtained by the ANN method show a better correlation with the experimental data than those obtained by the RSM method. This is corroborated in Fig. 7 which shows that the ANN model residues are much lower than those of RSM. This advantage of the ANN approach over its RSM counterpart can be explained by its efficiency in detecting non-linear relationships. It should, however, be noted that, in terms of identification and classification of the main factors and their significant interactions in the

model, the RSM method showed preeminence over the ANN approach. Therefore, and in order to establish a satisfying statistical study in terms of predictive modeling along with identifying the factors influencing the response investigated with their contributions, it is recommended to apply both ANN and RSM methods as they seem to be complementary.

5 Validation tests

The validation step is necessary to verifying the adequacy of the mathematical models derived by the RSM and ANN

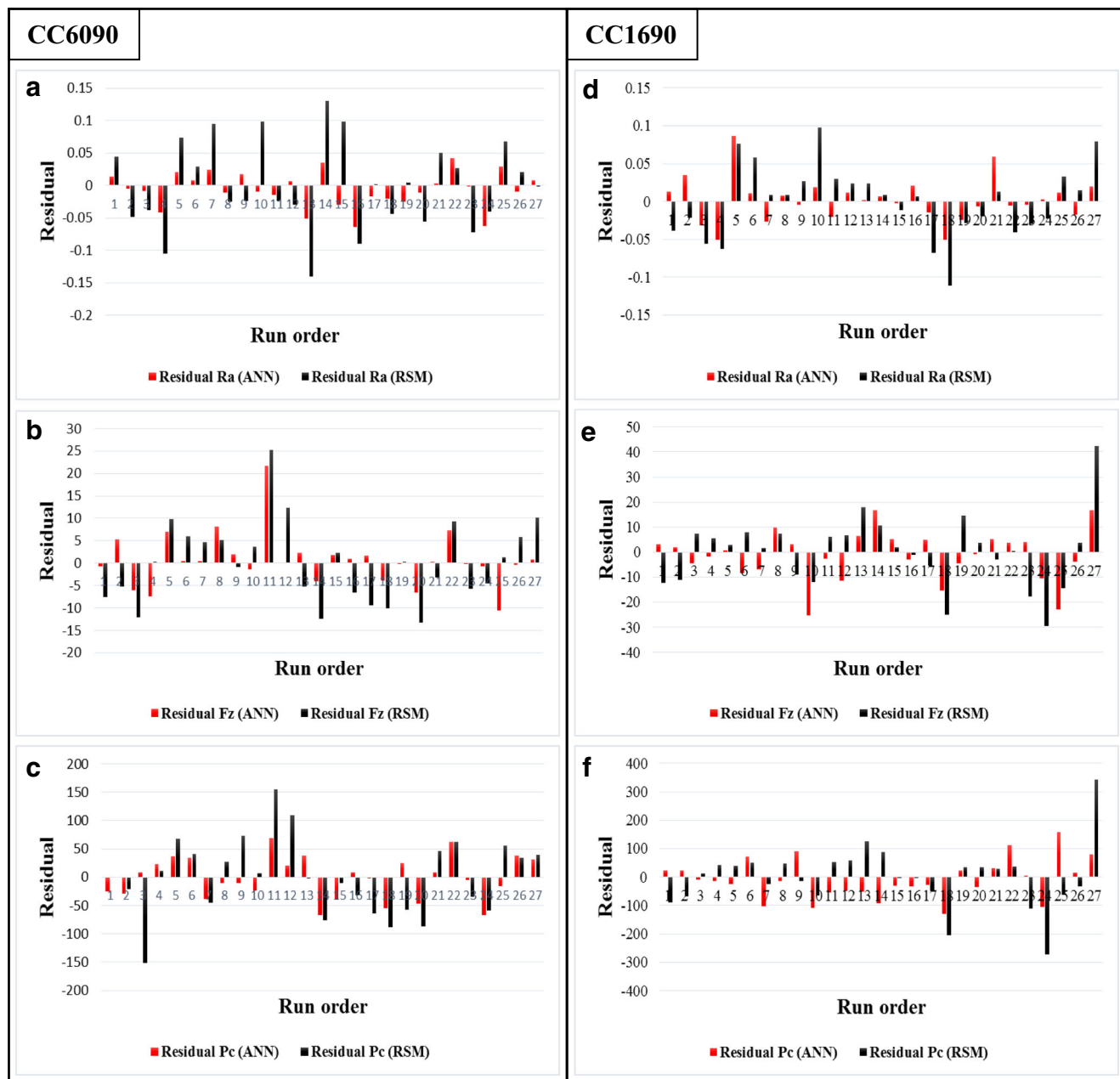


Fig. 7 Comparison between RSM and ANN model residues for Ra , F_z , and P_c

methods. This has been accomplished through carrying out four supplementary tests with cutting conditions that are different from those represented in Table 2. Figure 8a–c shows the results of these tests for the two ceramics. The results obtained show a tiny difference between the experimental and predicted values, especially for those predicted by ANN. Figure 11d–f represents the MAPE results of both the RSM and ANN methods obtained during the validation tests. According to these results, the errors pertaining to the RSM are found to be between (1.28 and 12)%, whereas those of the ANN rest in the range (0.53 and 6.13)%. The validation results achieved lead to confirm the consistency of the models derived by both ANN and RSM, and also to certify the

reliability of ANN models over those of RSM in terms of prediction. It is important to mention that the models developed are solely valid within the range of variation of the cutting conditions indicated in Table 2.

6 Optimization of cutting parameters

The multi-objective optimization implies the simultaneous optimization of several criteria at the same time even if they are contradictory, allowing to find out a compromise between various responses. Various optimization approaches are available, one of them being the genetic

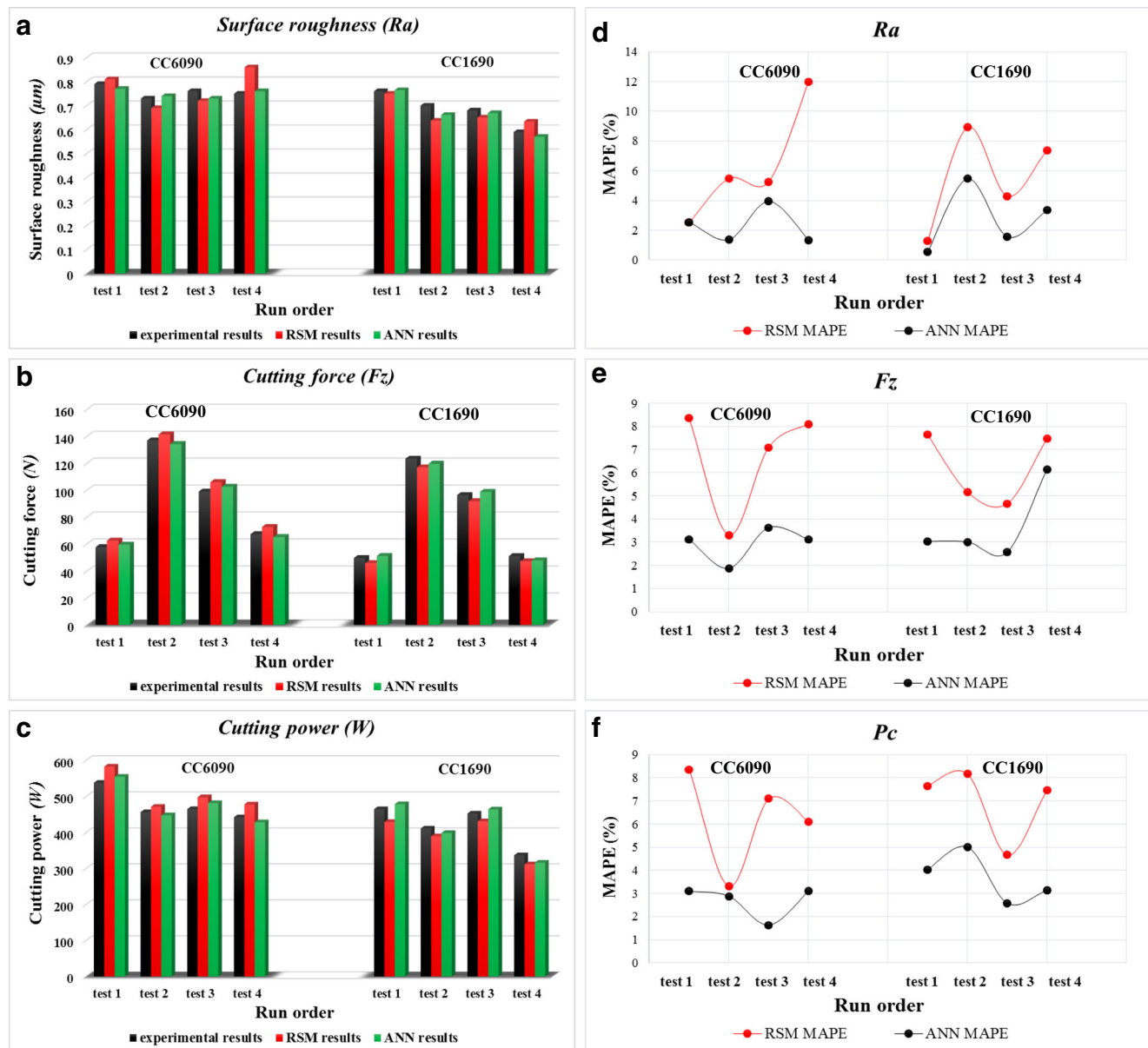


Fig. 8 Confirmation tests of the mathematical models of Ra , F_z , and P_c

algorithms (GA). They are essentially stochastic optimization algorithms based on the mechanisms of natural selection and genetics. Their application is extremely simple [32]. It starts with choosing a population of arbitrarily adopted initial potential solutions (chromosomes) whose relative performance (fitness) is evaluated. On the basis of the results obtained, a new population of potential solutions is developed using simple evolutionary operators such as selection, crossing, and mutation. This cycle is repeated until a satisfactory solution is found [33] (Fig. 9).

A genetic algorithm is mainly defined by its:

- Individual/chromosome/sequence: a potential solution to the problem
- Population: a set of chromosomes or points in the research space
- Environment: the research space
- Fitness function: the—positive—function we seek to maximize

Several research studies involving multi-criteria optimization problems and using GA are in progress. What differentiates the genetic algorithms from other optimization approaches may be summarized in four essential points:

- GA uses parameter coding and not the parameters themselves.
- GA works on a population of points and not on one particular point, thus enabling the research to be carried out on a multidimensional space.
- GA does not set any conditions on the nature of the functions to be optimized.

- GA uses probabilistic and non-deterministic transition rules.

6.1 The objective function

The present study performs a simultaneous minimization of the three criteria represented by R_a , F_z , and P_c , and tries to increase at the same time the material removal rate (MRR) for the two cutting materials tested (CC6090 and CC1690). It uses the genetic algorithm approach that is based on the mathematical models established by the ANN method due to the fact that it displayed better predictive potential that would lead to achieve the optimal cutting regimes. Genetic algorithms follow the principle of “survival of the fittest” that lead them to be naturally adapted to solving maximization problems and converting them into minimization ones through the application of a fitness function $F(x)$ that is a derivative of the objective function. The fitness function frequently used is of the form:

$$F(x) = \frac{1}{[1 + f(x)]} \quad (17)$$

Table 13 displays the cutting constraints adopted for the present case.

6.2 GA optimization results

6.2.1 Pareto front graphs

Optimizing engineering problems is a complex task as they are generally multi-objective and deal with parameters or

Fig. 9 Schematic diagram of a genetic algorithm

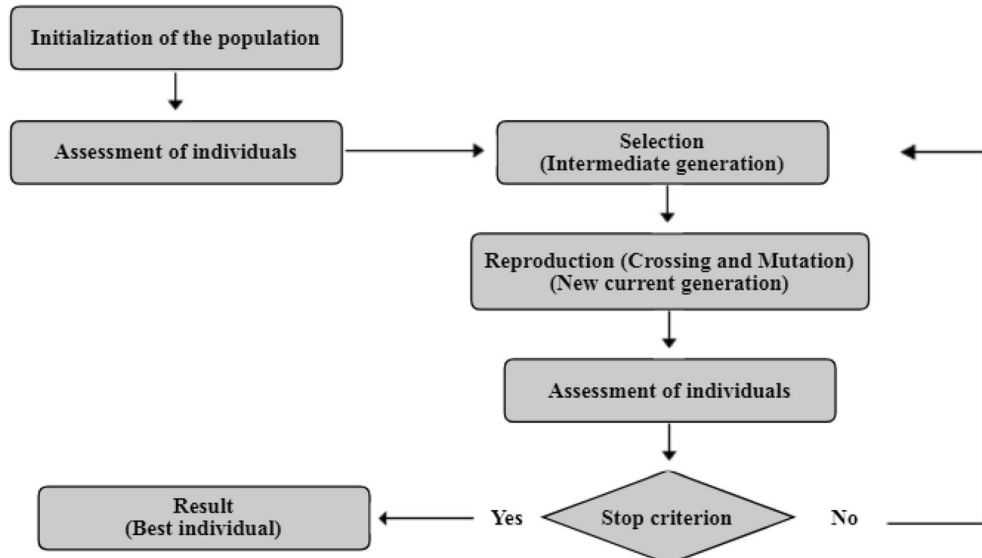
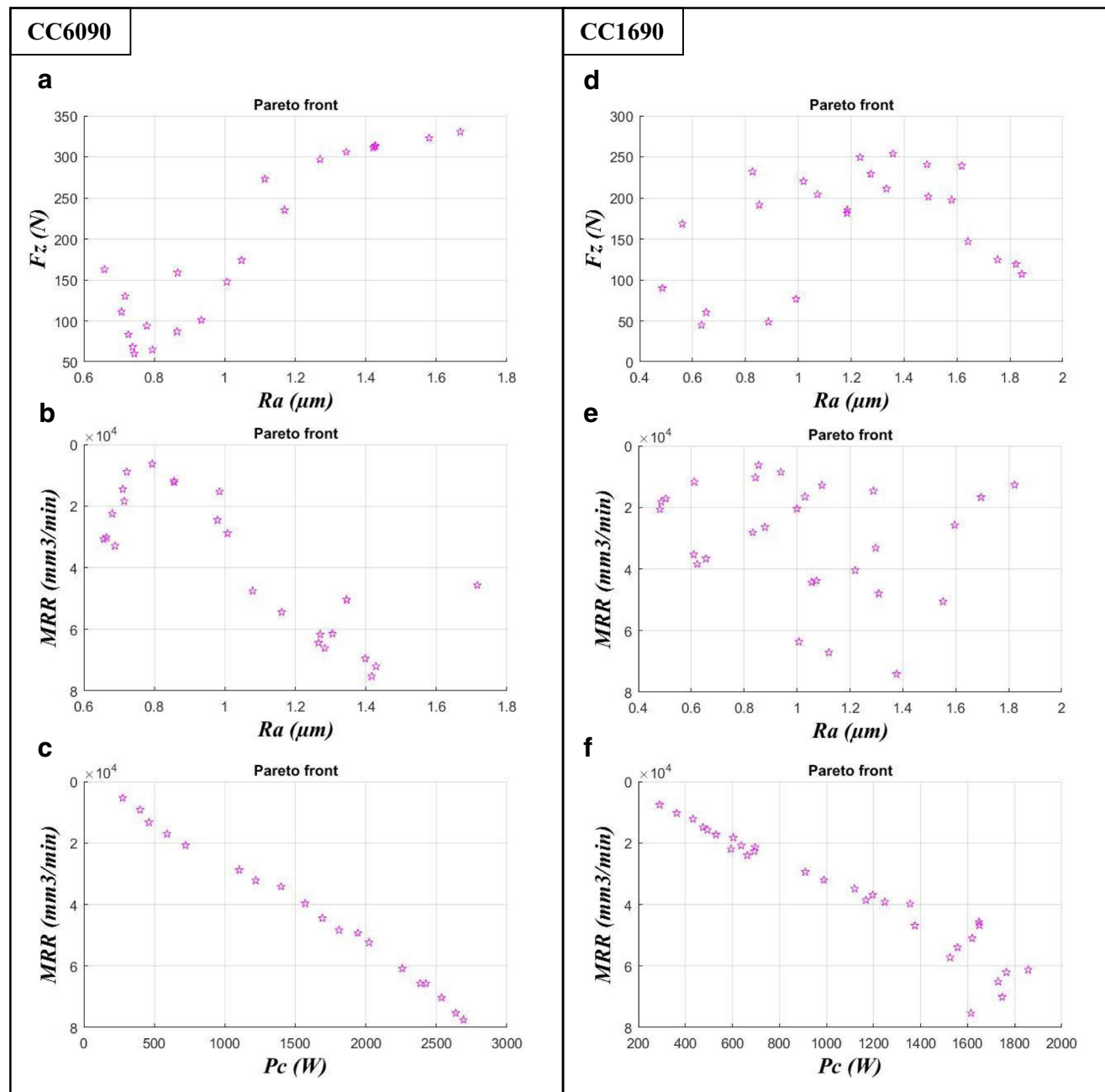


Table 13 Optimization conditions

Parameters	Objectives	Lower limit		Upper limit	
		CC6090	CC1690	CC6090	CC1690
V_c (m/min)	Gamme	260	260	530	530
f (mm/tr)	Gamme	0.08	0.08	0.2	0.2
a_p (mm)	Gamme	0.25	0.25	0.75	0.75
R_a (μm)	Min.	0.7	0.45	1.79	1.86
F_z (N)	Min.	54.9	30.37	349.77	307.73
P_c (W)	Min.	295.273	2710.68	197.513	1958.26
MRR (mm^3/min)	Max.	5200	79,500	5200	79,500

**Fig. 10** Pareto front graphs

loads that behave in a random manner. For these multi-objective problems, the solution can be presented as a Pareto front that helps the practitioner compromise between the different optimization criteria. Figure 10 shows the Pareto front graphs for the present optimization case. In this figure, the purple stars represent Pareto's optimal solutions. They are not affected by each other, as the minimum values of both the surface roughness and the cutting power correspond to small material removal rates. Therefore, there is no unique optimal solution but rather a set of optimal compromises,

and none of them can be identified as better than the others without preference information being included (constraints). It may be concluded that in fact, the choice of the optimal regime has to be adopted by the engineer himself.

6.2.2 Optimal cutting regimes

Table 14 presents the genetic algorithm optimization results for R_a , F_z , P_c , and MRR for the two cutting inserts. It shows that the cutting regimes adopted to obtain a compromise

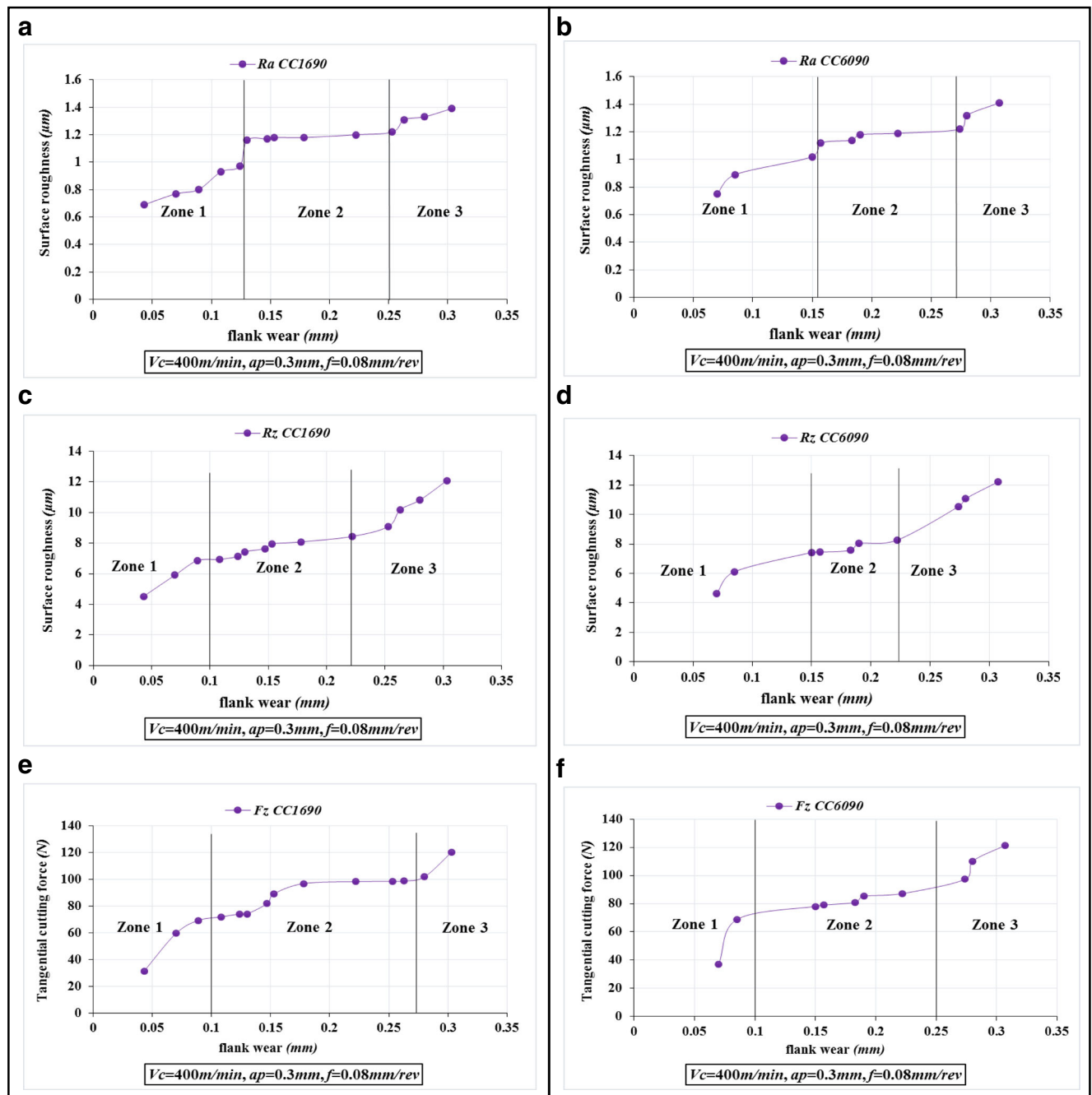


Fig. 11 Evolution of R_a and F_z as a function of machining time

between the four parameters correspond to the cutting condition ranges represented by ($V_c = 299.525\text{--}512.571 \text{ m/min}$, $f = 0.08\text{--}0.121 \text{ mm/rev}$, and $ap = 0.251\text{--}0.586 \text{ mm}$) for both ceramics.

7 Evolution of R_a , R_z , F_z , and V_b with machining time

Figure 11a–f displays the evolution of R_a , R_z , and F_z as a function of the flank wear (V_b). In this figure, all the curves show an ascending aspect meaning that the flank wear (V_b) possesses a significant effect on both the surface roughness and the cutting force.

Each of these curves can be divided into three zones in which the first shows the great influence of (V_b) on the variations of R_a , R_z , and F_z (i.e., the values of R_a , R_z , and F_z increase respectively with a rate of (47, 51, and 129)% for CC1690 and (49, 59, and 110)% for CC6090). The second zone displays more stable curves with small increases of (5, 23, and 37)% for CC1690 and (8.9, 11, and 11)% for the CC6090. In the third and last zone, another significant increase appears in terms of R_a , R_z , and F_z that reaches (14, 43, and 21)% for CC1690 and of (15.5, 47, and 43)% for CC6090. In summary, during the entire machining operation and with $V_b = 0.3 \text{ mm}$,

R_a , R_z , and F_z criteria have all increased from (0.79, 4.52, and 31.36) to (1.39, 12.09, and 120.23) for CC1690 ceramic which represents an increase of (76, 167, and 283)%, respectively. For the CC6090 ceramic, the increase was from (0.75, 4.65, and 37.091) to (1.41, 12.21, and 121.35) leading to a boost of (88, 162, and 227)%.

With the same cutting conditions and after 15 min of machining, the ratio $R_{a_{CC1690}}/R_{a_{CC6090}} = 0.88$, while $R_{z_{CC1690}}/R_{z_{CC6090}} = 0.87$ and $F_{z_{CC1690}}/F_{z_{CC6090}} = 0.94$. This leads to conclude that the coated ceramic (CC1690) performs better than the uncoated ceramic (CC6090) in terms of surface roughness and cutting force.

The deterioration of surface quality as a function of flank wear is a consequence of the damage to the cutting edge of the tool. The longer the edge is worn, the less sharp it becomes. This leads to a more frequent tearing of the workpiece's material that consequently prompts the degradation of the surface quality. Comparable results and comments are reported by Bouchelaghem and Yallese [26, 34].

The increase of the cutting force F_z with wear is the result of the increase of the contact surface between the tool and the workpiece that consequently lead to the augmentation of both the friction forces and the cutting force F_z . Similar results have been reported by Özel et al. [35, 36].

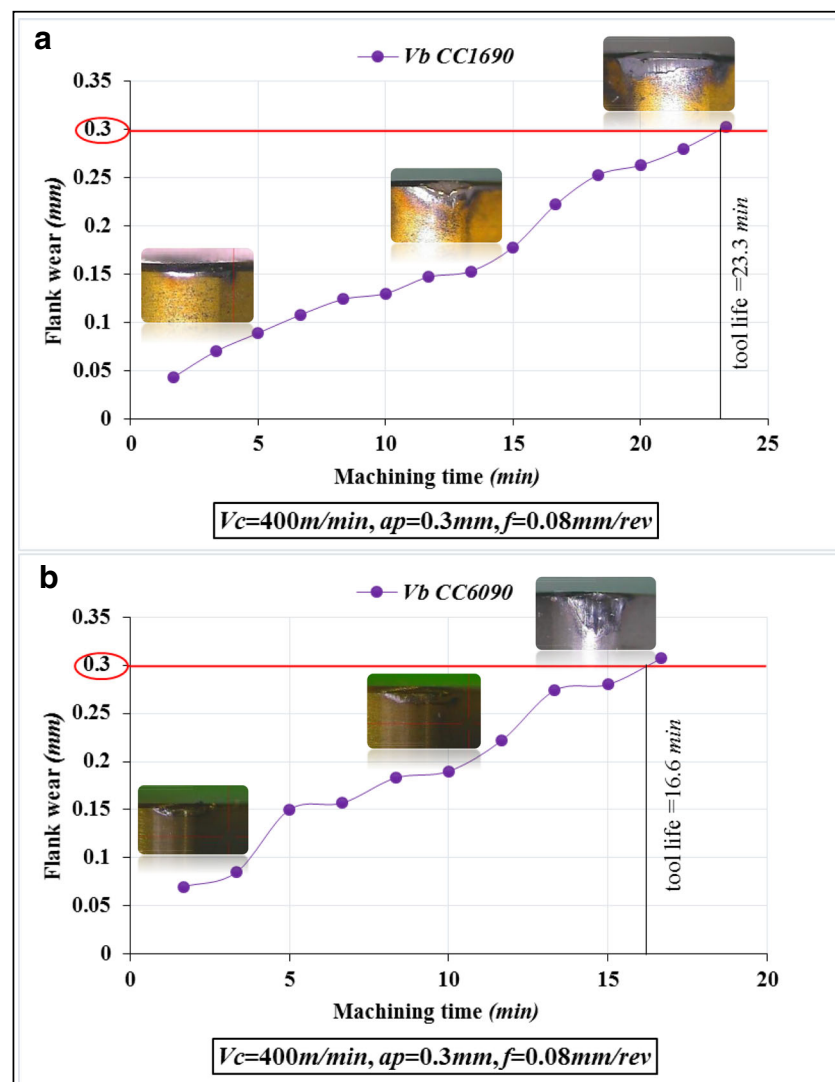
Figure 12a, b illustrates the evolution of the flank wear (V_b) with the machining time at $V_c = 400 \text{ m/min}$, $f =$

Table 14 Optimization results of GA function

No.	ap (mm)	f (mm/rev)	V_c (m/min)	R_a (μm)	F_z (N)	P_c (W)	MRR (mm^3/min)
CC6090							
1	0.544	0.107	503.504	0.660	156.932	1220.959	29,261.621
2	0.563	0.108	497.728	0.662	167.088	1272.612	30,325.622
3	0.586	0.087	500.334	0.692	141.763	1101.390	25,413.204
4	0.501	0.090	506.141	0.693	115.586	945.348	22,684.447
5	0.504	0.093	432.094	0.701	130.023	863.380	20,356.977
6	0.254	0.080	511.092	0.708	53.048	486.909	10,400.838
7	0.251	0.089	392.395	0.754	64.227	367.705	8811.109
8	0.268	0.090	329.573	0.798	71.250	353.245	7958.330
9	0.255	0.081	299.525	0.802	66.033	286.191	6188.744
10	0.251	0.089	323.298	0.814	68.569	326.842	7251.206
CC1690							
1	0.527	0.080	465.339	0.478	85.684	646.531	19,633.788
2	0.521	0.082	468.628	0.481	86.027	651.243	19,939.381
3	0.573	0.087	326.649	0.531	112.310	561.003	16,262.876
4	0.298	0.100	474.082	0.603	54.900	473.416	14,152.011
5	0.473	0.118	467.589	0.605	117.317	777.387	26,004.453
6	0.250	0.080	512.571	0.625	29.450	403.693	10,269.728
7	0.262	0.084	474.501	0.627	39.070	391.980	10,437.151
8	0.487	0.114	316.267	0.648	124.522	559.578	17,560.939
9	0.253	0.081	435.025	0.666	41.045	344.110	8892.198
10	0.551	0.121	315.014	0.679	153.821	682.955	21,019.595

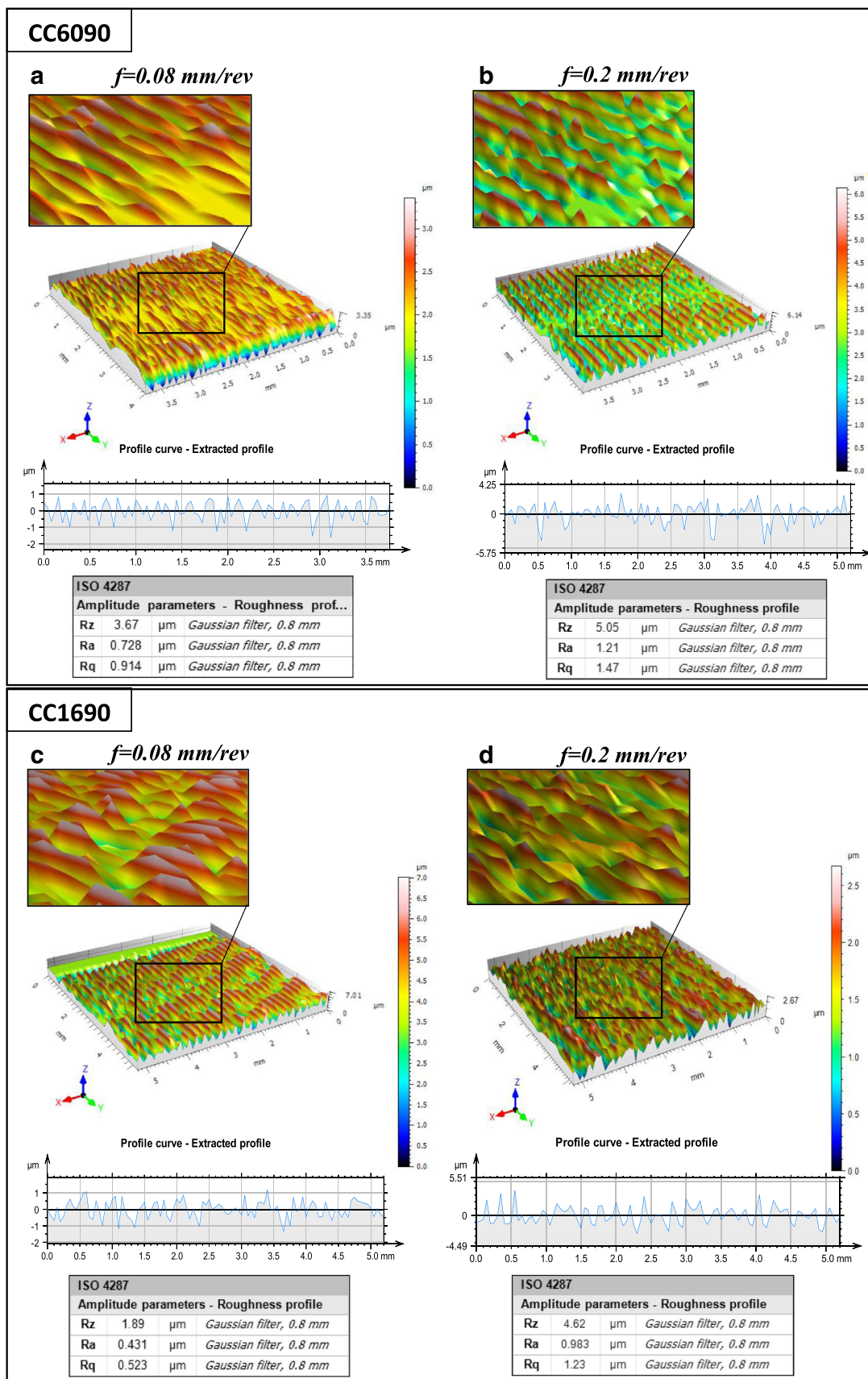
0.08 mm/rev, and $ap = 0.3$ mm for the two tested ceramics (CC1690 and CC6090). The results show that the increase in machining time generates an equal increase in flank wear for the two ceramics. As the tool works, the temperature at the interface tool/workpiece and tool/chip rises and consequently leads to an acceleration of abrasion and diffusion wear mechanisms [27, 37]. The admissible flank wear (V_b) is represented by a horizontal line whose intersection with the wear curve enables the determination of the strength of the two ceramics. Beyond $V_b = 0.3$ mm, wear increases sharply and the tool loses its cutting qualities, thus altering both the surface roughness and dimensional accuracy [38]. As a result, the coated ceramic tool reaches the admissible wear value of $V_b = 0.3$ mm after 23.3 min of machining time, while the uncoated ceramic tool reaches this value after only 16.6 min. The ratio of the tool life of CC1690 over that of CC6090 is found equal to 1.4. The superiority of the coated ceramic (CC1690) lies in fact on the coating layer (TiN) that gives the tool material better wear resistance [39].

Fig. 12 Evolution of V_b as a function of machining time for the CC6090 and CC1690 ceramics



8 3D surface topography

The 3D representation of the topography of the surfaces produced during the turning of the EN-GJL-250 Gy cast iron with the coated and uncoated silicon nitride ceramic using two different feed rates is shown in Fig. 13. It is noted that the generated surfaces are constituted by numerous interrupted corrugations that are the result of the presence of a high proportion of carbon (4%) in the form of very hard lamellar graphite that leads to the weakening of the cast iron structure and the damage of the whole surface. Other researchers [5, 6, 40] have analyzed the 3D surface topography of the steel workpiece and found that the profile obtained was continuous and does not show any damaged ridges. Moreover, the grooves generated are found to be deeper and wider along with the distance between peaks and valleys which is found to be important when the feed rate varies between 0.08 and 0.2 mm/rev. Finally and for $f = 0.08$ mm/rev, $R_a_{CC1690} = 0.431 \mu\text{m}$, and $R_a_{CC6090} = 0.728 \mu\text{m}$, the coated ceramic

**Fig. 13** 3D surface topography

(CC1690) presents a lower roughness criterion than that of the uncoated ceramic (CC6090). The superiority of the CC1690 ceramic may be explained by its coating layer that leads to the reduction of the coefficient of friction between the cutting tool and the workpiece, and consequently that of the cutting forces leading to the improvement of the surface quality [41]. Similar results were found by Sharif et al. [42].

9 Conclusions

The statistical and modeling investigations carried out on R_a , F_z , and P_c using both the RSM and ANN methods along with the optimization of the cutting parameters using genetic algorithms (GA), and finally the wear tests and analysis of the surface topography (3D) of the gray cast iron EN-GJL-250 machined by silicon nitride ceramics (Si_3N_4) coated and uncoated (CC6090 and CC1690) lead to the following conclusions:

1. The ANOVA shows that:
 - (a) The feed rate affects the roughness considerably with contributions between (65 and 74)% for CC6090 ceramic and (73 and 86)% for CC1690. It is followed by the cutting speed with contributions between (12 and 15)% and (3 and 10)%; and the depth of cut that comes in third position with contributions of (2.5 and 4.5)% and (3.3 and 7.7)%.
 - (b) The cutting force is largely influenced by the cutting depth followed by the feed rate and the cutting speed with contributions of (64.73 and 69.63)%, (20.09 and 22.78)%, and (1.3 and 4.28)%, respectively. The ($ap \times f$) interaction is also found to be significant with a contribution of (1.45 and 3.74)%.
 - (c) All cutting parameters (i.e., V_c , f , and ap) along with all interactions have an impact on P_c , the depth of pass showing the greatest influence with a contribution of (57.71 and 61.87)%. It is followed by the feed rate with a contribution of (18.76 and 17.71)%, and finally, the cutting speed with a contribution of (16.4 and 11.75)%.
 - (d) The three cutting regime elements and all their interactions have a significant effect on MRR. The depth of cut comes first with a contribution of 41.45% followed by the feed rate (30.45%) and finally the cutting speed (19.48%).
2. The mathematical models developed for R_a , F_z , and P_c using the RSM and ANN methods are very useful for prediction purposes. A close correlation between the predicted and measured data was found with (R^2) varying between (0.95 and 0.99).
3. The comparison between ANN and RSM techniques shows that the ANN approach is more efficient in terms of predictive capacity than the RSM method, this latter being more useful in terms of identifying the cutting parameters and their interactions which influence the investigated responses.
4. Validation tests performed on the different prediction models developed by ANN and RSM confirm their capabilities when applied to predicting R_a , F_z , and P_c criteria.
5. The results derived from the genetic algorithm (GA) optimization application show that the cutting regimes adopted to obtaining a compromise between R_a , F_z , P_c , and MRR correspond to the following cutting condition ranges: ($V_c = 299.525\text{--}512.571$ m/min, $f = 0.8\text{--}0.121$ mm/rev, $ap = 0.251\text{--}0.586$ mm) for both ceramics investigated.
6. The analysis of the results shown in Table 3 leads to conclude that CC1690 ceramic performs better in terms of surface roughness and cutting force than its CC6090 ceramic counterpart. The R_a roughness criterion did not exceed 0.93 μm for CC6090 ceramic and 0.86 μm for its corresponding CC1690 ceramic for $f = 0.08$ mm/rev and at different V_c and ap .
7. For both ceramics (CC1690 and CC6090), the behavior of roughness, cutting force, and wear with the machining time show that at the same cutting conditions and after 15 min of machining, the ratios $R_a_{CC1690}/R_a_{CC6090} = 0.88$ and $F_z_{CC1690}/F_z_{CC6090} = 0.94$. Moreover, when the flank wear reaches the admissible value of $V_b = 0.3$, the ratio tool life $CC1690/\text{tool life } CC6090$ is found to equal 1.4.
8. The modular optical metrology platform is an important investigation tool in the analysis of surface roughness. It helped understand the characteristics of EN-GJL-250 gray cast iron machined surfaces.
9. The visualization of the surfaces 3D topography shows that the surfaces generated on the EN-GJL-250 cast iron are constituted of many interrupted ridges.

Nomenclature V_c , cutting speed (m/min); ap , depth of cut (mm); f , feed rate (mm/rev); ANN, artificial neural network; GA, genetic algorithm; HRC, rockwell hardness; HB, Brinell hardness; ANOVA, analysis of variance; SC, square sum; MC, mean of the sum of the squares; DF, degrees of freedom; Cont. %, contribution ratio (%); P_c , cutting power (W); R^2 , coefficient of determination (%); R_a , arithmetic mean roughness (μm); RSM, response surface methodology; V_b , flank wear (mm)

Publisher's Note Springer Nature remains neutral with regard to jurisdictional claims in published maps and institutional affiliations.

References

1. Özel T, Karpat Y (2005) Predictive modeling of surface roughness and tool wear in hard turning using regression and neural networks. Int J Mach Tools Manuf 45(4–5):467–479

2. Tapoglou N, Lopez MIA, Cook I, Taylor CM (2017) Investigation of the influence of CO₂ cryogenic coolant application on tool wear. *Procedia CIRP* 63:745–749
3. Danish M, Ginta TL, Habib K, Abdul Rani AM, Saha BB (2018) Effect of cryogenic cooling on the heat transfer during turning of AZ31C magnesium alloy. *Heat Transfer Eng* 1–10. <https://doi.org/10.1080/01457632.2018.1450345>
4. Bensouilah H, Aouici H, Meddour I, Yallese MA, Mabrouki T, Girardin F (2016) Performance of coated and uncoated mixed ceramic tools in hard turning process. *Measurement* 82:1–18
5. Nouioua M, Yallese MA, Khettabi R, Belhadi S, Mabrouki T (2017) Comparative assessment of cooling conditions, including MQL technology on machining factors in an environmentally friendly approach. *Int J Adv Manuf Technol* 91(9–12):3079–3094
6. Khellaf A, Aouici H, Smaiah S, Boutabba S, Yallese MA, Elbah M (2017) Comparative assessment of two ceramic cutting tools on surface roughness in hard turning of AISI H11 steel: including 2D and 3D surface topography. *Int J Adv Manuf Technol* 89(1–4):333–354
7. Ho WH, Tsai JT, Lin BT, Chou JH (2009) Adaptive network-based fuzzy inference system for prediction of surface roughness in end milling process using hybrid Taguchi-genetic learning algorithm. *Expert Syst Appl* 36(2):3216–3222
8. Kumaran S, Jesuthanam CP, Kumar RA (2008) Application of multiple regression and adaptive neuro fuzzy inference system for the prediction of surface roughness. *Int J Adv Manuf Technol* 35(7–8):778–788
9. Maher I, Eltaib MEH, Sarhan AA, El-Zahry RM (2014) Investigation of the effect of machining parameters on the surface quality of machined brass (60/40) in CNC end milling—ANFIS modeling. *Int J Adv Manuf Technol* 74(1–4):531–537
10. Maran JP, Sivakumar V, Thirugnanasambandham K, Sridhar R (2013) Artificial neural network and response surface methodology modeling in mass transfer parameters predictions during osmotic dehydration of Carica papaya L. *Alex Eng J* 52(3):507–516
11. Nouioua M, Yallese MA, Khettabi R, Belhadi S, Bouhalais ML, Girardin F (2017) Investigation of the performance of the MQL, dry, and wet turning by response surface methodology (RSM) and artificial neural network (ANN). *Int J Adv Manuf Technol* 93(5–8):2485–2504
12. Hossain MSJ, Ahmad N (2014) Surface roughness prediction modelling for commercial dies using ANFIS, ANN and RSM. *Int J Ind Syst Eng* 16(2):156–183
13. Kamruzzaman M, Rahman SS, Ashraf MZI, Dhar NR (2017) Modeling of chip-tool interface temperature using response surface methodology and artificial neural network in HPC-assisted turning and tool life investigation. *Int J Adv Manuf Technol* 90(5–8):1547–1568
14. Yücel E, Güney M (2013) Modelling and optimization of the cutting conditions in hard turning of high-alloy white cast iron (Ni-hard). *Proc Inst Mech Eng C J Mech Eng Sci* 227(10):2280–2290
15. Fetecau C, Stan F (2012) Study of cutting force and surface roughness in the turning of polytetrafluoroethylene composites with a polycrystalline diamond tool. *Measurement* 45(6):1367–1379
16. Zhong ZW, Khoo LP, Han ST (2006) Prediction of surface roughness of turned surfaces using neural networks. *Int J Adv Manuf Technol* 28(7–8):688–693
17. Mia M, Dhar NR (2016) Response surface and neural network based predictive models of cutting temperature in hard turning. *J Adv Res* 7(6):1035–1044
18. Chabbi A, Yallese MA, Nouioua M, Meddour I, Mabrouki T, Girardin F (2017) Modeling and optimization of turning process parameters during the cutting of polymer (POM C) based on RSM, ANN, and DF methods. *Int J Adv Manuf Technol* 91(5–8):2267–2290
19. Tebassi H, Yallese MA, Meddour I, Girardin F, Mabrouki T (2017) On the modeling of surface roughness and cutting force when turning of Inconel 718 using artificial neural network and response surface methodology: accuracy and benefit. *Period Polytech Mech Engrg* 61(1):1–11
20. Danish M, Ginta TL, Habib K, Carou D, Rani AMA, Saha BB (2017) Thermal analysis during turning of AZ31 magnesium alloy under dry and cryogenic conditions. *Int J Adv Manuf Technol* 91(5–8):2855–2868
21. Yousuff CM, Danish M, Ho ETW, Kamal Basha IH, Hamid NHB (2017) Study on the optimum cutting parameters of an aluminum mold for effective bonding strength of a PDMS microfluidic device. *Micromachines* 8(8):258
22. Kumar R, Chauhan S (2015) Study on surface roughness measurement for turning of Al 7075/10/SiCp and Al 7075 hybrid composites by using response surface methodology (RSM) and artificial neural networking (ANN). *Measurement* 65:166–180
23. D'Addona DM, Raykar SJ (2016) Analysis of surface roughness in hard turning using wiper insert geometry. *Procedia CIRP* 41: 841–846
24. Lin WS, Lee BY, Wu CL (2001) Modeling the surface roughness and cutting force for turning. *J Mater Process Technol* 108(3):286–293
25. Yallese MA, Boulanouar L, Chaoui K (2004) Usinage de l'acier 100Cr6 trempé par un outil en nitride de bore cubique. *Mechanics Industry* 5(4):355–368
26. Bouchelaghem H, Yallese MA, Amirat A, Belhadi S (2007) Wear behaviour of CBN tool when turning hardened AISI D3 steel. *Mechanics* 65(3):57–65
27. Yallese MA, Chaoui K, Zeghib N, Boulanouar L, Rigal JF (2009) Hard machining of hardened bearing steel using cubic boron nitride tool. *J Mater Process Technol* 209(2):1092–1104
28. Bouzid L, Yallese MA, Chaoui K, Mabrouki T, Boulanouar L (2015) Mathematical modeling for turning on AISI 420 stainless steel using surface response methodology. *Proc Inst Mech Eng B J Eng Manuf* 229(1):45–61
29. Elbah M, Yallese MA, Aouici H, Mabrouki T, Rigal JF (2013) Comparative assessment of wiper and conventional ceramic tools on surface roughness in hard turning AISI 4140 steel. *Measurement* 46(9):3041–3056
30. Singh KP, Basant A, Malik A, Jain G (2009) Artificial neural network modeling of the river water quality—a case study. *Ecol Model* 220(6):888–895
31. Feng CX (2001) An experimental study of the impact of turning parameters on surface roughness. In Proceedings of the industrial engineering research conference (Vol. 2036)
32. Saravanan RSRS, Sankar RS, Asokan P, Vijayakumar K, Prabhaharan G (2005) Optimization of cutting conditions during continuous finished profile machining using non-traditional techniques. *Int J Adv Manuf Technol* 26(1–2):30–40
33. Reddy NSK, Rao PV (2005) Selection of optimum tool geometry and cutting conditions using a surface roughness prediction model for end milling. *Int J Adv Manuf Technol* 26(11–12):1202–1210
34. Yallese MA, Rigal JF, Chaoui K, Boulanouar L (2005) The effects of cutting conditions on mixed ceramic and cubic boron nitride tool wear and on surface roughness during machining of X200Cr12 steel (60 HRC). *Proc Inst Mech Eng B J Eng Manuf* 219(1):35–55
35. Öznel T, Karpat Y, Figueira L, Davim JP (2007) Modelling of surface finish and tool flank wear in turning of AISI D2 steel with ceramic wiper inserts. *J Mater Process Technol* 189(1–3):192–198
36. Öznel T, Nadgir A (2002) Prediction of flank wear by using back propagation neural network modeling when cutting hardened H-13 steel with chamfered and honed CBN tools. *Int J Mach Tools Manuf* 42(2):287–297
37. Bouchelaghem H, Yallese MA, Mabrouki T, Amirat A, Rigal JF (2010) Experimental investigation and performance analyses of CBN insert in hard turning of cold work tool steel (D3). *Mach Sci Technol* 14(4):471–501
38. Aouici H, Yallese MA, Fnides B, Chaoui K, Mabrouki T (2011) Modeling and optimization of hard turning of X38CrMoV5-1 steel with CBN tool: machining parameters effects on flank wear and surface roughness. *J Mech Sci Technol* 25(11):2843–2851

39. Sahoo AK, Sahoo B (2012) Experimental investigations on machinability aspects in finish hard turning of AISI 4340 steel using uncoated and multilayer coated carbide inserts. *Measurement* 45(8):2153–2165
40. Meddour I, Yallese MA, Khattabi R, Elbah M, Boulanouar L (2015) Investigation and modeling of cutting forces and surface roughness when hard turning of AISI 52100 steel with mixed ceramic tool: cutting conditions optimization. *Int J Adv Manuf Technol* 77(5–8):1387–1399
41. Swain N, Venkatesh V, Kumar P, Srinivas G, Ravishankar S, Barshilia HC (2017) An experimental investigation on the machining characteristics of Nimonic 75 using uncoated and TiAlN coated tungsten carbide micro-end mills. *CIRP J Manuf Sci Technol* 16:34–42
42. Sharif S, Rahim EA (2007) Performance of coated-and uncoated-carbide tools when drilling titanium alloy—Ti–6Al4V. *J Mater Process Technol* 185(1–3):72–76